PROPERTIES OF

α-MONOCLINIC SELENIUM

Thesis by

Joseph Dean Taynai

In Partial Fulfillment of the Requirements

For the Degree of

Doctor of Philosophy

California Institute of Technology

Pasadena, California

1970

(Submitted November 18, 1969)

ACKNOWLEDGEMENTS

For their guidance, patience, and encouragement, I am deeply indebted to Dr. Marc-A. Nicolet and Dr. Carver Mead. I sincerely thank Mr. Sigeru Iizima for all his work in initiating the selenium project, Dr. John Caywood for his help in much of the optical work, and Mr. Kim Mitchell for his assistance in many tasks. For their helpful discussions, I thank Drs. Richard Marsh, Sten Samson, G. Wilse Robinson, and Robert Langmuir.

The selenium, provided by the Selenium-Tellurium Development Association, is very much appreciated. Fellowship assistance from the Fairchild Camera and Instrument Corp., the California State Scholarship and Loan Commission, the General Telephone and Electronics Laboratories, the National Science Foundation and the Ford Foundation are greatfully acknowledged, as well as research support from the National Aeronautics and Space Administration and the Jet Propulsion Laboratory.

For her great patience and encouragement, I thank my wife, Marilyn. Finally, for her assistance as secretary and typist, I thank Miss Carolyn Elsbree.

ABSTRACT

The growth of bulky and platelet shaped α-monoclinic crystals is discussed. A simple method is devised for identifying and orienting them.

The density, previously in disagreement with the value calculated from x-ray studies, is carefully redetermined, and found to be in good agreement with the latter.

The relative dielectric constant is determined, an effort being made to eliminate errors inherent in previous measurements, which have not been in agreement. A two parameter model is derived which explains the anisotropy in the relative dielectric constant of orthorhombic sulfur, which is also composed of 8-atom puckered ring molecules. The model works less well for α-monoclinic selenium. The relative dielectric constant anisotropy is quite noticeable, being 6.06 along the crystal b axis, and 8.52 - 8.93 normal to the axis.

Thin crystal platelets of α-monoclinic selenium (less than 1μ thick) are used to extend optical transmission measurements up to 4.5eV. Previously the measurements extended up to 2.1 eV, limited by the thickness of the available crystals. The absorption edge is at 2.20 eV, with changes in slope of the absorption coefficient occurring at 2.85 eV and 3.8 eV. Measurement of transmission through solutions of selenium in CS_2 and trichlorethylene yield an absorption edge of 2.75 eV. There is evidence the selenium exists in solution partly as Se_8 rings, the building block of monoclinic selenium. Transmission is measured at

low temperatures (80^{o}K and 10^{o}K) using the platelets. The absorption edge is at 2.38 eV and 2.39 eV, respectively, for the two temperatures. Measurements at low temperatures with polarized and unpolarized light reveal interesting absorption anisotropy near 2.65 eV.

TABLE OF CONTENTS

CHAPTER IV

OPTICAL ABSORPTION

INTRODUCTION

Solid selenium is known to exist in four different modifications: trigonal (also called metallic, hexagonal, grey), amorphous (including vitreous), α-monoclinic and β-monoclinic. The element was discovered by Berzelius in 1818, but it was not until 1855 that Mitscherlich reported monoclinic selenium, and not until 1890 that Muthmann distinguished between the α and β modifications.

The electrical and optical properties of the α-monoclinic form were first investigated by Gudden and Pohl, and by Kyropoulos in the middle 1920's. In the late 1950's, Prosser developed crystal growing techniques and extended optical measurements. Finally, in late 1966, Iizima began to work on the material, concerning himself mainly with electrical properties.

The work reported here contains some careful redeterminations of previously reported results, some obvious extensions of previous work, and some new investigations.

Chapter I deals with crystal growth and identification. The work of Chapter II is a careful redetermination of the density of α-monoclinic selenium, previous experimental densities being in disagreement with the density calculated from x-ray data. Chapter III describes a determination of the dielectric constant and its anisotropy, and presents a simple model for it based on orthorhombic sulfur. Chapter IV describes optical transmission measurements made on α-monoclinic crystals at room temperature and low temperatures, and on selenium dissolved in solvents.

Also, polarization dependence of the absorption coefficient is studied and discussed.

CHAPTER I

CRYSTAL GROWTH AND IDENTIFICATION

1.1 Crystal Growth

Properties of crystalline materials can best be investigated using large single crystals relatively free from defects. Monoclinic selenium cannot easily be obtained in this condition. It cannot be grown from a melt or from a vapor, since these techniques will only yield trigonal crystals. However, monoclinic crystals can be grown from a saturated solution. This technique is somewhat hampered by the low solubility of selenium[1.1] in most solvents (see Table 1.1). Since Mitscherlich[1.2] discovered monoclinic selenium in 1856, crystals of the α and β modifications have been grown almost exclusively from a saturated solution of selenium in carbon disulfide (CS_2). Selenium is also reported[1.3] to be soluble in H_2SO_4 and HNO_3. However, no crystals have been grown from solutions using these two as solvents.

1.1.1 Growth of Bulky Crystals

Two methods have been employed for growing monoclinic selenium crystals. The first is evaporation of a saturated solution of selenium in CS_2. Muthmann[1.4] describes production of both α- and β- monoclinic crystals by slow and rapid evaporation respectively. Unfortunately, the crystals produced in this manner are quite small, less than a millimeter across.

TABLE 1.1

SOLUBILITY OF α-MONOCLINIC SELENIUM

IN VARIOUS SOLVENTS AT 27°C

Solvent	Chemical Formula	Solubility of Selenium (weight percent)
Methylene Iodide	CH_2I_2	0.36
Carbon Disulfide	CS_2	0.055
Ethyl Iodide	CH_3CH_2I	0.0080
Trichlorethylene	$CHCl:CCl_2$	0.0016
Chloroform	$CHCl_3$	0.0010
Carbon Tetrachloride	CCl_4	0.000

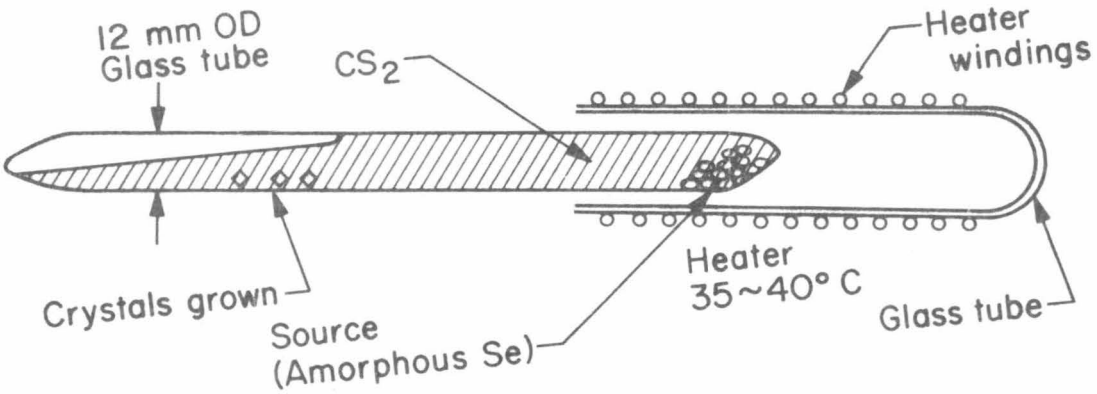

Figure 1.1 Apparatus for growing bulky α-monoclinic selenium crystals.

The second method is a continuous process which utilizes the difference in solubility of selenium in CS_2 at different temperatures (Fig. 1.1). Amorphous selenium is placed at the source end of a long tube which is then filled with CS_2 and sealed. A temperature gradient is applied by heating the source end by placing it in a resistance heater. The solubility of selenium in CS_2 increases with increasing temperature[1.1]. Thus, the CS_2 at the warm source end dissolves and maintains more selenium in solution than the CS_2 at the cool end. Selenium is transported from the warm to the cool end by diffusion and convection. The resulting supersaturated solution at the cool end precipitates selenium. A few large monoclinic crystals develop if the tube is very clean, the ambient and heater temperatures are held constant, and the solvent and solute are of high purity. To aid the development of a few large crystals, the cool end can be seeded with a few small α-monoclinic crystals (see Fig. 1.1).

Optimal results are obtained with an ambient temperature of $20^{\circ}C$ and a source end temperature of about $37^{\circ}C$. Reagent grade CS_2 is used. Amorphous selenium in pellet form was supplied by Canadian Copper Refining Ltd. (Hyperpure Se) and Gallard-Schleisinger Co. (99.9999% Se). The crystals take 3-9 weeks to grow to millimeter size. Sudden downward changes in ambient or source end temperature cause many small crystals to nucleate, preventing development of large crystals. Placing the apparatus in a constant temperature chamber prevents this.

The crystals obtained were α-monoclinic (see Section 1.2), ranging in size from microscopic to about 3mm across. Drawings[1.5] of typical

crystals are shown in Fig. 1.2. They are called bulky crystals, to distinguish them from the very thin ones described in the next section.

1.1.2 Growth of Crystal Platelets

Very thin crystals are grown by evaporating a small amount of selenium-saturated CS_2 on a clean substrate (usually glass or quartz). These platelets usually are hexagonally shaped (Fig. 1.3) and are several hundred microns across. Measured thicknesses range from 0.07μ to 0.8μ. Thicker platelets have been observed, but they have not been of uniform thickness.

Substrates with areas of about 5 cm^2 work well. Smaller substrates do not yield large platelets, since there is insufficient selenium available in the reduced amount of solution which can be placed on a smaller substrate. Growing crystals using larger substrates, accomodating more solution, produces small bulky crystals and thick, irregular platelets.

The rate of evaporation has a great effect upon the size of the platelets. By restricting the air flow near the substrate with a cover glass, the evaporation time, which is 2-3 minutes with no cover, can be increased to several hours. The largest crystals are obtained when the evaporation time is about 30 minutes, for a 2.5 cm diameter substrate whose upper surface only is covered with the solution (Fig. 1.4).

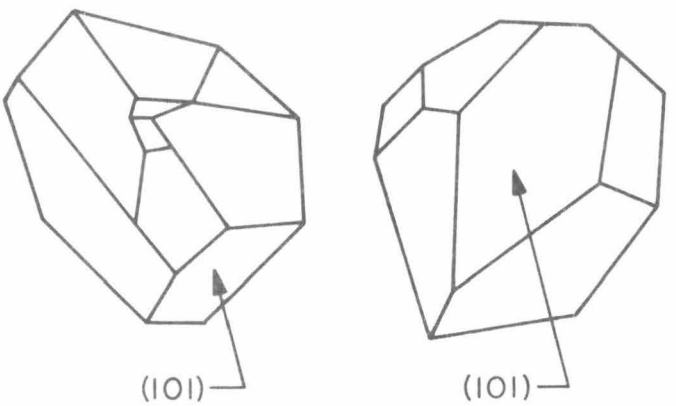

Figure 1.2 Typical habits of α-monoclinic selenium crystals. The (101) faces are usually the most well developed ones.

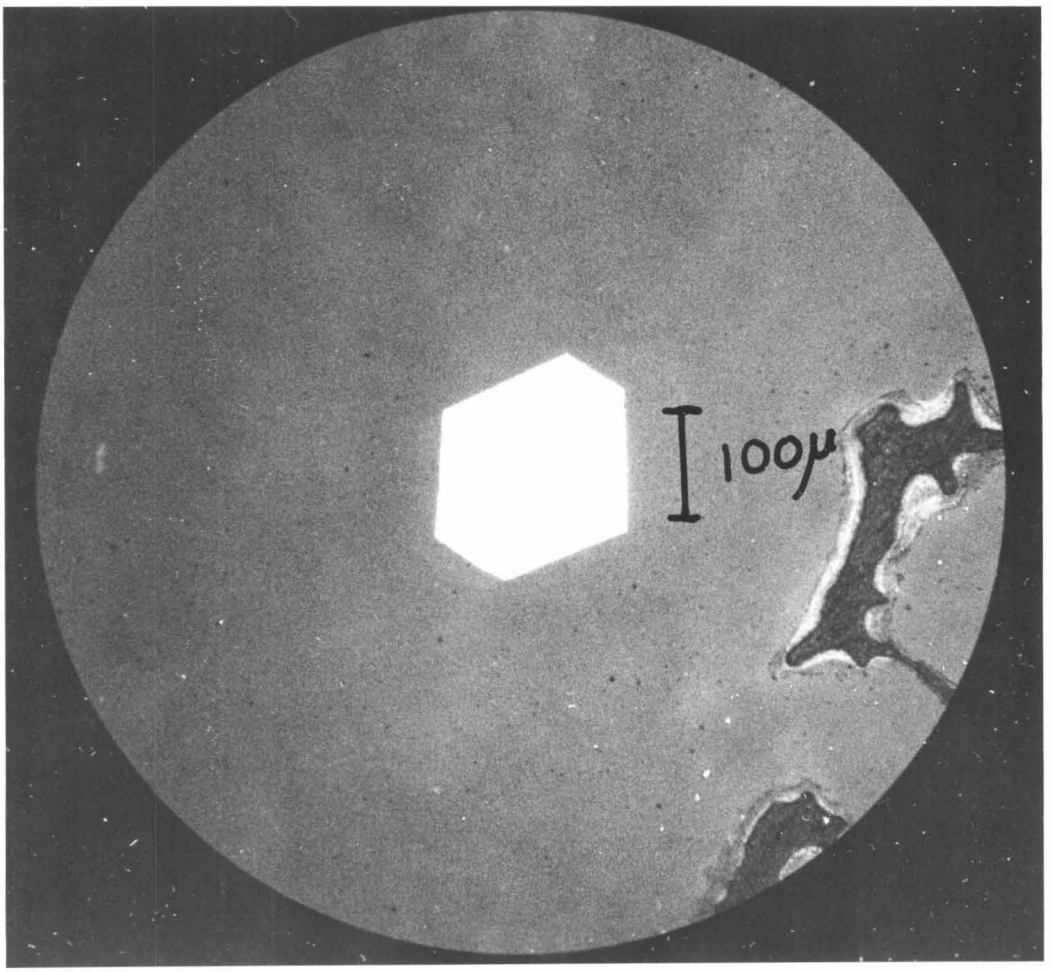

Figure 1.3 A photomicrograph of a typical platelet of α-monoclinic selenium. Over 100μ across, it is about 0.5μ thick.

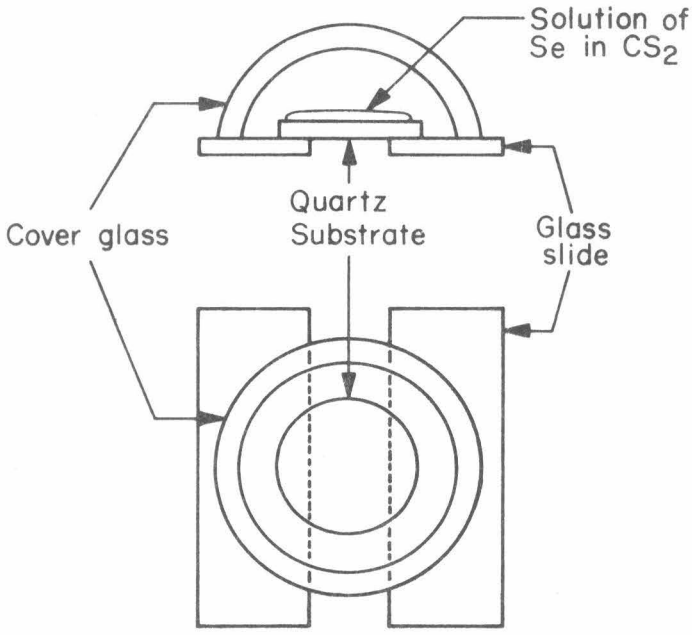

Figure 1.4 Apparatus for growing platelet crystals of α-monoclinic selenium.

1.2 Identification and Orientation of Crystals

After the crystals were first grown, their crystal type had to be determined. Then a method had to be found to determine the orientation of the crystal. Both these problems could be solved by doing an X-ray determination of the unit cell parameters and crystal axis directions of a mounted crystal. However, this is laborious and time consuming to do for many crystals. Rather than doing an X-ray determination for each crystal, a simple method of orientation was sought. Then the X-ray determination could be performed on a few crystals to verify the simple method.

The crystals (bulky crystals and platelets) had to be monoclinic, since they dissolved in CS_2, while the trigonal form is relatively insoluble[1.1] in the liquid. However, the α- and β-monoclinic modifications are not easily differentiated. Both consist of unit cells containing four 8-atom rings, in slightly different orientations[1.6,1.7]. The unit cell parameters are given in Table 1.2.

To identify a crystal from its habit, a crystal face must first be identified, then the angles bounding the face measured. These measured values can then be compared with the values calculated from the α- and β-monoclinic cell dimensions for the identified face. Klug[1.8] maintains microscopic observation is insufficient to distinguish between the two varieties. This is not true if the correct face is chosen. Mitscherlich[1.2] and Muthmann[1.4] state that the principal faces (marked (101) in Fig. 1.2) are (101) planes, usually intersected by $(10\bar{1})$, (110), and (011) planes for α-monoclinic crystals and $(10\bar{1})$,

TABLE 1.2

STRUCTURAL DATA FOR α- AND β-MONOCLINIC SELENIUM[1.6, 1.7]

Crystal	Cell Dimensions	Cell Content	Space Group
α-monoclinic	a = 9.05 ± .01 A	32 atoms	$p2_1/n$
	b = 9.07 ± .01 A		
	c = 11.61 ± .01 A		
	$\beta = 90^{\circ}\ 46' \pm 5'$		
β-monoclinic	a = 12.85 ± .01 A	32 atoms	$p2_1/a$
	b = 8.07 ± .01 A		
	c = 9.31 ± .01 A		
	$\beta = 93^{\circ}\ 8' \pm 5'$		

$(12\bar{1})$, and $(\bar{1}21)$ planes for β-monoclinic crystals (The crystallographic notations refer to the unit cells of Burbank[1.6] and Marsh[1.7].). Assuming these observations to be true, the angles bounding the (101) plane can be calculated from the data in Table 1.2 and the crystal planes involved. These calculated angles are shown in Table 1.3.

The platelets were hexagonal, and six angles could be measured. The principal faces of the bulky crystals were rhombus shaped, and only two obtuse angles could be measured. If the principal faces of the crystals were indeed (101) planes, a microscope which could distinguish between 116^{o} 22 1/2' and 117^{o} 3' would certainly be sufficient.

Using a Leitz-Wetzlar microscope with a calibrated rotating stage, angles could be measured within 10' of arc. A X10 eyepiece and X3.8, X11, and X32 objective lenses were used, depending on crystal size. Angles were measured on 7 platelets, 42 angles in all. On each platelet, a pair of opposite angles was near 117^{o}, the other four near 121 $1/2^{o}$. Nine angles were measured on bulky crystals. The results appear in Table 1.4. Thus, from Tables 1.3 and 1.4, the crystals appear to be α-monoclinic.

However, in addition to demonstrating the existence of a correlation between *calculated* and measured angles, uniqueness also had to be shown. Many different combinations of crystal planes may yield almost identical angles. Thus, angles were calculated for combinations of as many crystal planes as seemed feasible. The total number of ways, NT, to choose a base plane and two intersecting planes (all different) from a set of N planes is:

TABLE 1.3

ANGLES BOUNDING THE (101) FACE FOR

α- AND β-MONOCLINIC SELENIUM

Crystal	Angle	Planes
α-monoclinic	121° 28 1/2'	$(10\bar{1})$ and (110)
	121° 28 1/2'	$(10\bar{1})$ and $(1\bar{1}0)$
	117° 3'	(110) and $(1\bar{1}0)$
β-monoclinic	116° 22 1/2'	$(10\bar{1})$ and $(12\bar{1})$
	116° 22 1/2'	$(10\bar{1})$ and $(\bar{1}21)$
	127° 15'	$(12\bar{1})$ and $(\bar{1}21)$

TABLE 1.4

ANGLES BOUNDING PRINCIPAL FACES

ON MONOCLINIC SELENIUM CRYSTALS

Crystal Type	Number of Angles	Angle
Platelet	14	116° 59' ± 11'
	28	121° 39' ± 11'
Bulky Crystal	9	117° 6' ± 10'

$$NT = N(N-1)(N-2)/2 \qquad (1.1)$$

Using planes with Miller indices containing 0, 1 and -1, N = 13, NT = 858. For planes with indices containing 2, 1, 0, -1 and -2, N = 49, NT = 55,696. The first is not unmanageable if done on a computer; the second is unwieldy in any case (A listing of the program used is found in Appendix A.). For the α-monoclinic parameters, the planes used were (100), (010), (001), (110), $(1\bar{1}0)$, (101), $(10\bar{1})$, (011), $(01\bar{1})$, (111), $(11\bar{1})$, $(1\bar{1}1)$, $(\bar{1}11)$. In addition, for the β-monoclinic parameters, the (121), $(12\bar{1})$, $(\bar{1}21)$, and $(\bar{1}2\bar{1})$ planes were used, since Muthmann[1.4] considered them likely.

The table of angles generated by the computer program in Appendix A shows that there are no other likely candidates for crystal planes which yield comparable angles among the low order planes used. At this point, it seemed expedient to have these results verified, rather than continue by looking for higher order planes. Dr. Richard Marsh[1.9], using X-rays, verified the crystals were α-monoclinic, and the principal face on the crystals tested was the (101) plane. The results also showed a high degree of lattice perfection. The lattice constants determined agree with those given by Burbank[1.5] for α-monoclinic selenium.

1.3 Crystal Imperfection and Damage

Large bulky crystals often contain voids. Sometimes these are obvious from external deformations observed. Internal imperfections can often be discovered by observing with a microscope the light

transmitted through the crystal. Uniform light intensity across a crystal face indicates a void free crystal.

For many measurements, crystals must be polished parallel to a known crystal plane. From polishing a large number of crystals, these observations have been made:

1. Crystals over 2mm across usually contain voids.
2. Crystals with poorly developed faces, or jagged edges usually contain voids.
3. Crystals under 2mm across with well developed faces are usually free of voids.

Platelets can be checked easily. Being very thin, imperfections can be clearly seen with a microscope. Uniformity of thickness can be checked with a phase contrast microscope (a Reichert (Austria)). The actual thickness, in addition to the uniformity, was measured using interferometric techniques (see Section 4.2.1).

CHAPTER II

DENSITY

The α-monoclinic modification of selenium is composed of puckered rings of 8 atoms each, 4 rings to the unit cell. The crystallographic parameters have been measured quite accurately[2.1]:

$$a = 9.05 \pm .01 \text{ A}$$

$$b = 9.07 \pm .01 \text{ A}$$

$$c = 11.61 \pm .01 \text{ A}$$

$$\beta = 90^{\circ}\ 46' \pm 5'$$

where a, b, c are the lengths of the three axes of the unit cell and β is the angle between the non-orthogonal axes. The volume of the unit cell is:

$$\begin{aligned} v &= a \cdot b \cdot c \cdot \sin (90^{\circ}\ 46') \\ &= 9.529 \pm .029 \times 10^{-22} \text{ cm}^3 \end{aligned} \tag{2.1}$$

The weight of the atoms in the unit cell is 32 x 78.96 amu (the atomic weight of selenium), which is $4.1938 \pm .0005 \times 10^{-21}$ g/unit cell. The density is simply given by this weight divided by the volume of the unit cell (Eq. 2.1):

$$\rho = w/v = 4.401 \pm .016 \text{ g/cm}^3 \tag{2.2}$$

The crystals used were grown[2.2] from a solution of selenium dissolved in CS_2. Densities were determined for amorphous and α-monoclinic selenium. Each density was determined by 4 weighings on an analytic chain balance, whose error was $\pm$ .2 mg.

The method used was that of displacement weighing. The weighing flask was suspended empty in air and weighed (w_1). Next, the flask was immersed in a liquid and weighed (w_2). Third, the flask was dried, filled with selenium, suspended in air and weighed (w_3). Finally, the filled flask was immersed in the liquid (Fig. 2.1) and weighed (w_4).

$$w_1 = w_g - \rho_a v_g \tag{2.3a}$$

$$w_2 = w_g - \rho_L(T_1) v_g \tag{2.3b}$$

$$w_3 = w_g + w_{Se} - \rho_a (v_g + v_{Se}) \tag{2.3c}$$

$$w_4 = w_g + w_{Se} - \rho_L(T_2)\ (v_g + v_{Se}) \tag{2.3d}$$

w_g and w_{Se} are the weights of the glass weighing flask and the selenium respectively. Similarly, v_g and v_{Se} are the respective volumes. $\rho_L(T_1)$ and $\rho_L(T_2)$ are the densities of the liquid at the temperatures T_1 and T_2 respectively. Since the temperature was not maintained constant, it was recorded at each weighing. ρ_a is the density of air.

Defining:

$$\rho_{Se} = w_{Se}/v_{Se} \tag{2.4}$$

and solving (2.3) we have:

$$\rho_{Se} = \frac{(w_3 - w_1)}{(w_3 - w_4)/(\rho_L(T_2) - \rho_a) - (w_1 - w_2)/(\rho_L(T_1) - \rho_a)} + \rho_a \tag{2.5}$$

The error in ignoring ρ_a is less than 10^{-3}, yielding:

$$\rho_{Se} = \frac{}{(w_3 - w_4)/\rho_L(T_2) - (w_1 - w_2)/\rho_L(T_1)} \tag{2.6}$$

The small glass weighing flasks were blown from 2mm i.d. pyrex glass tubing. For small quantities of material, sturdy flasks were made weighing less than 0.3 g which held over 1 g of material. They were suspended from the balance by a human hair, which was thin enough to displace very little liquid, and weighed about 1 mg. Carbon tetrachloride (CCl_4) was chosen as the liquid for several reasons. First, selenium is insoluble[2.3] in it. Second, its viscosity is low and it wets glass and selenium, virtually eliminating trapped air bubbles. Third, CCl_4 is relatively dense, making $(w_3 - w_4)$ significant in Eq. (2.6). Fourth, it is readily available in high purity. Fifth, its density as a function of temperature is accurately known. Its disadvantage is its high rate of evaporation at room temperature, creating thermal gradients in the bath. To combat this, the CCl_4 surface was covered by a thin layer of ethylene glycol, which has a very low vapor pressure. It is less dense than CCl_4 and the two liquids are immiscible. Thus, the ethylene glycol prevents evaporative cooling, stabilizing the temperature of the bath (see Fig. 2.1).

The density of the CCl_4 as a function of temperature was taken from ref. 2.4. A linear fit was made to the data:

$$\rho_L(T) = 1.5940 - .00192 \cdot (T - 20) \quad 15 \leq T \leq 25 \qquad (2.7)$$

where T is the liquid temperature in degrees Centigrade and ρ_L is the density of the CCl_4.

The four weights were correct to within 0.2 mg, out of approximately 300, 100, 1100, and 600 mg for w_1, w_2, w_3, and w_4 respectively. The

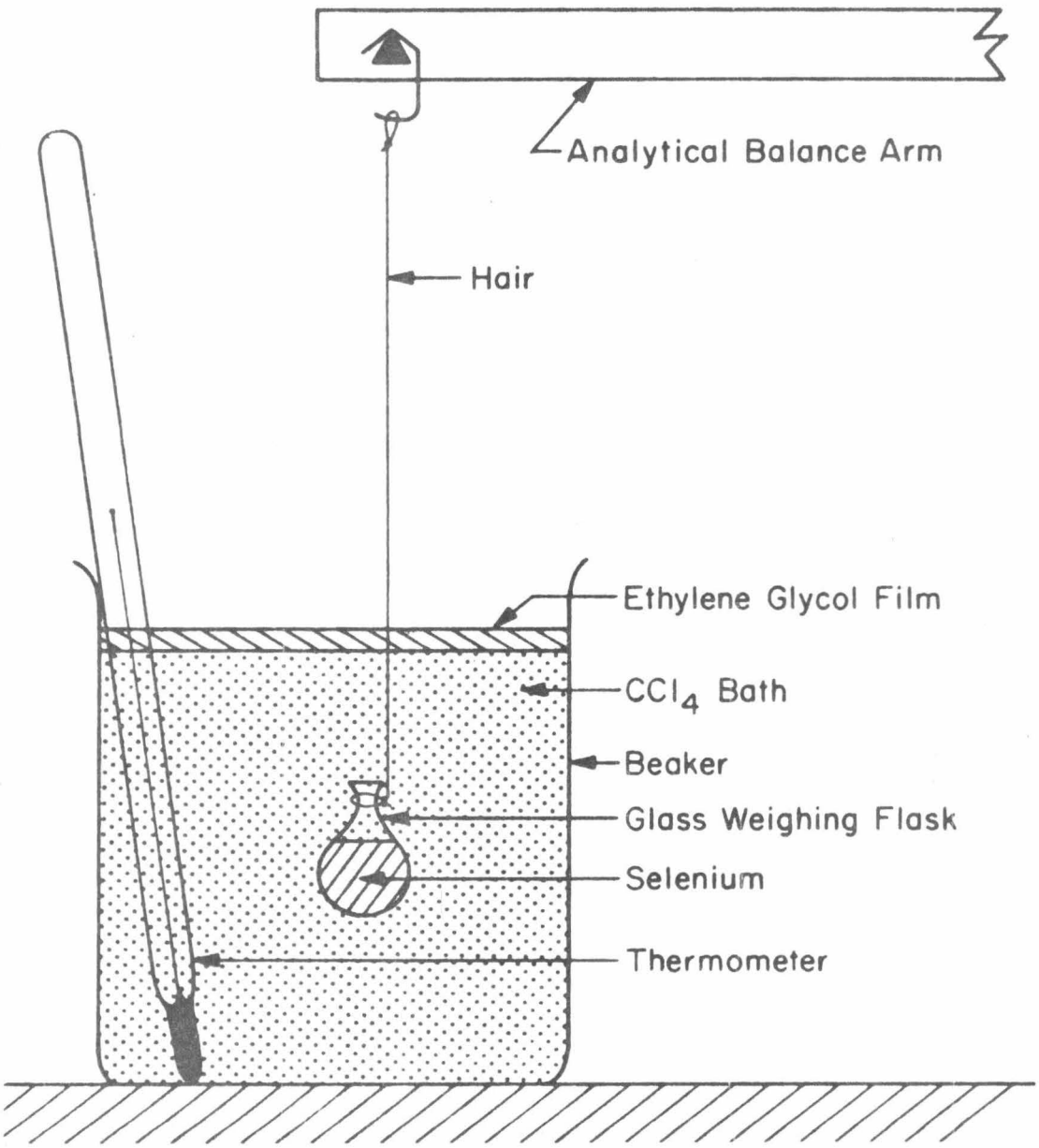

Figure 2.1 Apparatus for density measurements.

temperature was known to within $0.1^{o}C$. The error due to thermal expansion of the glass flasks was less than 10^{-4} for maximum temperature fluctuations observed. The estimated overall experimental error was approximately 0.3%.

Density measurements were made on amorphous and α-monoclinic selenium (whole and finely crushed crystals). The results are given in Table 2.1. The results show that the method gives the accepted value for the density of amorphous selenium, and the new experimental density for α-monoclinic selenium (finely crushed crystals) agrees well within experimental error with the density calculated from X-ray data. However, the density for the whole crystals is about 0.8% low, indicating the presence of some voids, even in the small crystals used for these measurements.

The published density values[2.6 - 2.11] range from 4.44 to 4.51 g/cm^3. These are unreasonably high, compared with the calculated value of 4.40 g/cm^3. The α-monoclinic form of selenium is metastable, however, and converts irreversibly to the higher density trigonal form ($\rho \simeq 4.8$ g/cm^3). The conversion will take place at room temperature over a period of a few years[2.12]. Heating will accelerate the process[2.13]. It seems likely that the previous density measurements were made on partially converted material.

TABLE 2.1

CALCULATED AND EXPERIMENTAL DENSITIES

OF AMORPHOUS AND α-MONOCLINIC SELENIUM

Crystal Modification	Density (g/cm^3) Experimental	Calculated	Literature[2.5]
amorphous	4.265 ± .014	-	4.26
α-monoclinic (whole)	4.353 ± .015	4.401 ± .016	4.50
α-monoclinic (crushed)	4.389 ± .015	4.401 ± .016	4.50

CHAPTER III

DIELECTRIC CONSTANT AND ANISOTROPY

3.1 Introduction

The dielectric constant of α-monoclinic selenium has not previously been satisfactorily determined. Earlier results are found in Table 3.1. The lack of agreement alone is sufficient reason to justify a careful determination. The problems encountered by the three investigators should be considered, so their errors might be avoided.

Gudden and Pohl[3.4], using crystals supplied by Kyropoulos for photoconductivity work, report that the crystals were porous. Iizima's[3.5] determination is questionable because of geometry considerations. He calculated the dielectric constant using the parallel plate capacitor approximation:

$$C = \epsilon_r \epsilon_o A / t \qquad (3.1)$$

where C is the capacitance, ϵ_r is the relative dielectric constant, ϵ_o is the permittivity of free space, A is the area of the capacitor plates, and t is the crystal thickness. This approximation is only valid for $t \ll \sqrt{A}$, since this minimizes the effect of fringing fields where the capacitor plates end. This was not true for Iizima's samples. Caywood used relatively void free crystals and geometry for which Equation 3.1 was valid. However, he used gold contacts evaporated directly on the selenium crystal. Iizima[3.5] noticed that such an operation changes the appearance of the selenium directly under the

TABLE 3.1

PREVIOUS DIELECTRIC CONSTANT MEASUREMENTS

ON α-MONOCLINIC SELENIUM

Dielectric Constant	Crystal Direction	Researcher
7.39	unspecified	Kyropoulos (3.1)
6.5 ± 0.6	[101]	Iizima (3.2)
9.2 ± 0.6	[101]	Caywood (3.3)

evaporated contact (discovered by mechanically polishing away the evaporated contact). The altered region may be one of three things:

1. A layer of trigonal selenium, converted from the α-monoclinic by thermal energy from the gold vapor during evaporation.
2. A gold-selenium alloy.
3. A gold-selenium compound.

Conversion is known to occur upon application of heat[3.6], and is probably the best explanation. Gold and selenium have not been successfully alloyed[3.7], and it is doubtful there was sufficient thermal energy involved in the evaporation to produce Au_2Se_3, the only reported gold-selenium compound.

In addition to these problems, α-monoclinic selenium is a very difficult material to which to make good electrical contact. Selenium appears to react[3.3, 3.5] with most of the materials (aluminum, gallium, nickel, silver) which were used to contact it. Also the crystals are quite fragile and shatter when handled roughly or when cleaving is attempted.

Summarizing the restrictions:

1. The crystals must be free of voids.
2. Geometry must be considered carefully if the dielectric constant is to be calculated from a geometric model, since the crystals are quite small and some assumptions may be violated.
3. Intimate electrical contact can not be made by any method yet attempted.
4. The crystals are fragile, and must not be roughly handled.

Finally, the crystal is monoclinic. Therefore, α-monoclinic selenium may exhibit anisotropy in the dielectric constant (see Section 3.2.2).

3.2 Derivations

Section 3.2.1, Dielectric Constant Derivation and Error Analysis, and Section 3.3, Experimental Apparatus, are presented separately. However, the work of the two sections was simultaneous, and much of what was learned in one caused changes in the other as the work progressed.

The Dielectric Anisotropy Model, Section 3.2.2, was derived because of the similarity between orthorhombic sulfur and α-monoclinic selenium. The measured[3.8] dielectric constant anisotropy of sulfur can be accurately explained by the model. The similarity between the sulfur and selenium forms indicate the model may also work for selenium. The model predicts a greater anisotropy for α-monoclinic selenium than for orthorhombic sulfur, which should be measurable by the method of Sections 3.2.1 and 3.3.

3.2.1 Dielectric Constant Derivation and Error Analysis

The apparatus used for the dielectric constant measurement (Fig. 3.1 and Section 3.3) is approximated by a parallel plate capacitor partially filled with a dielectric slab (Fig. 3.2). This may be simply treated as an air capacitor and a dielectric (selenium) filled capacitor in series. Eq. 3.1 becomes:

$$C_{Se} = \epsilon_{Se}\ \epsilon_o\ A\ /t \qquad (3.2a)$$

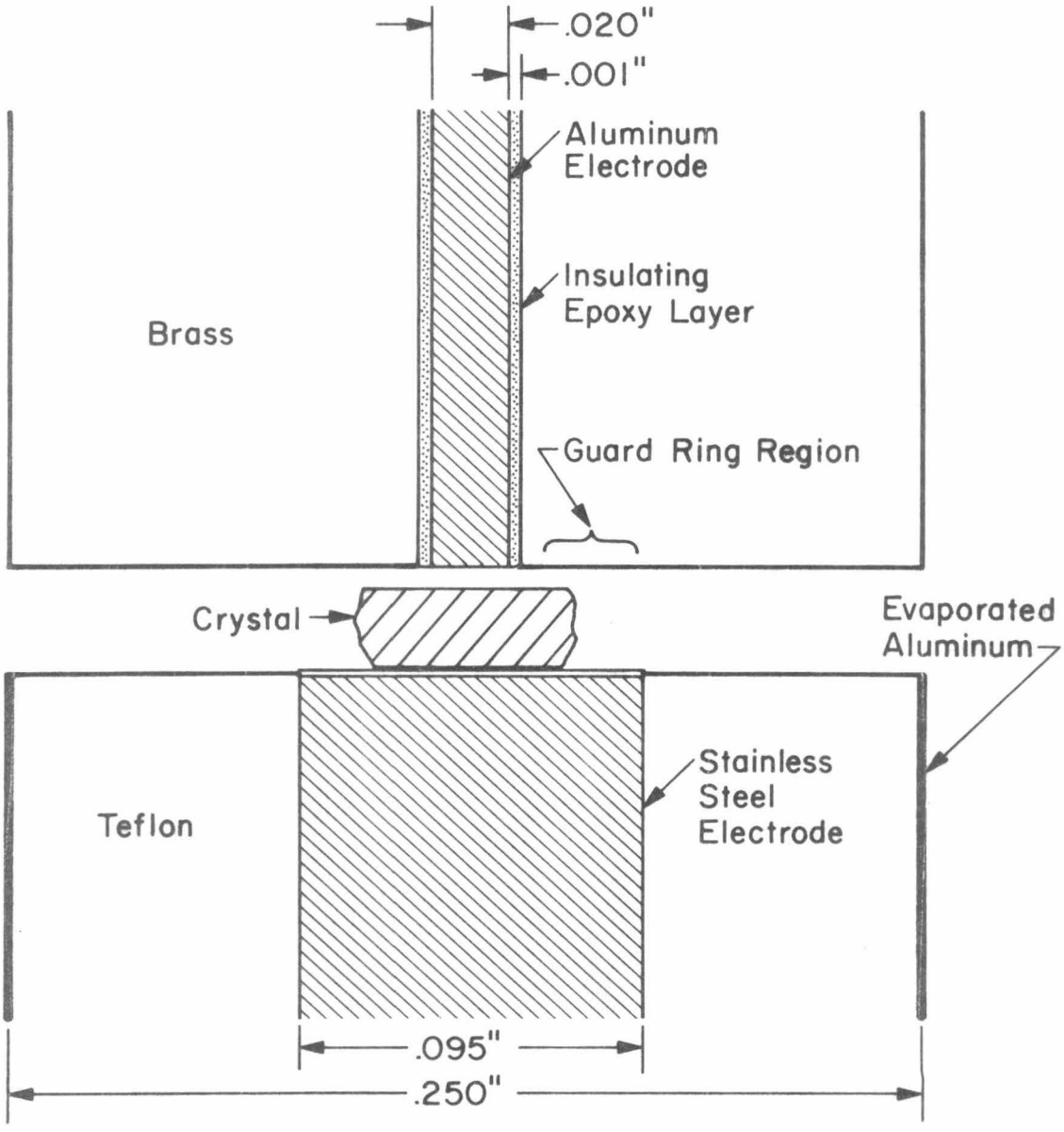

Figure 3.1 Apparatus for dielectric constant measurement. The upper electrode is movable vertically. The structure is cylindrical about the vertical axis.

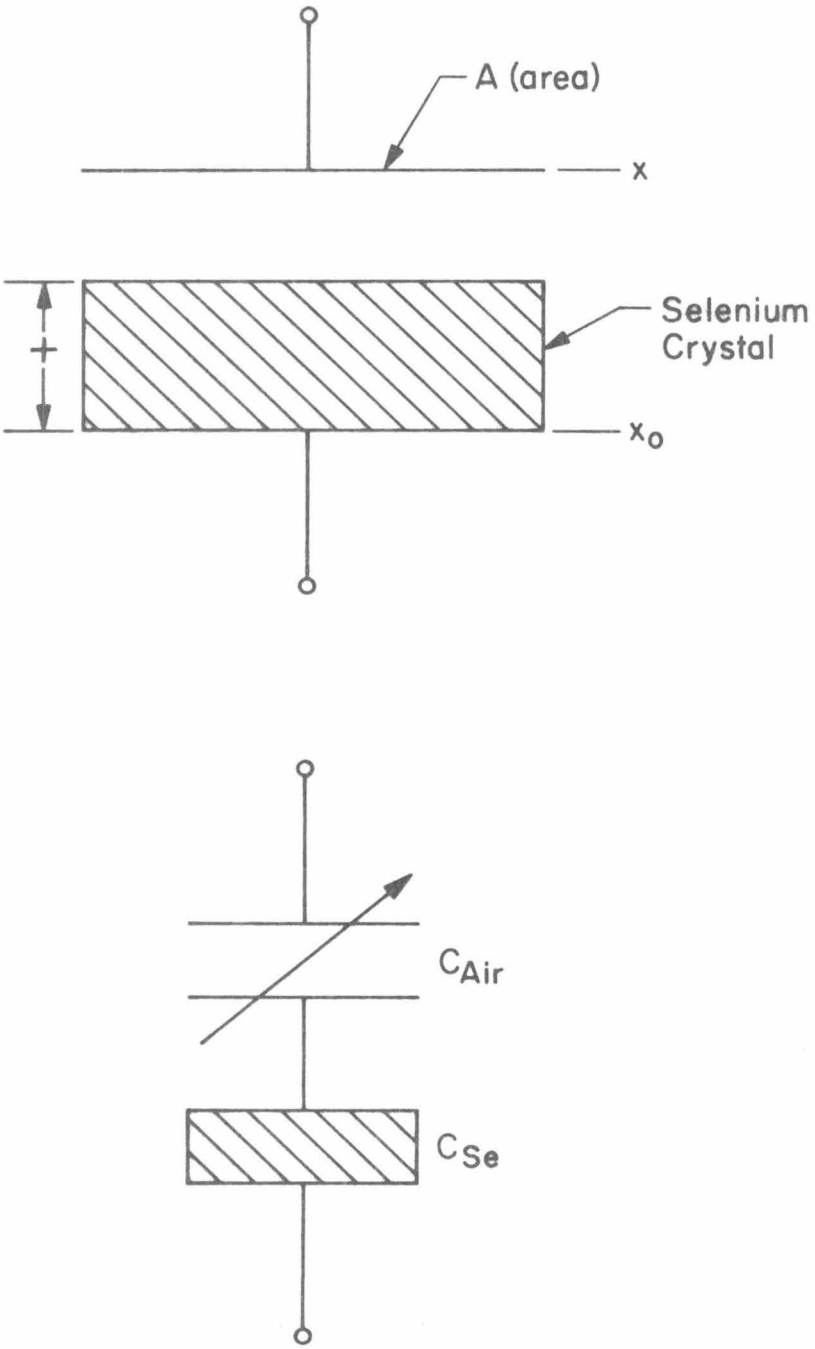

Figure 3.2 Approximation of the dielectric constant measurement apparatus.

$$C_{Air} = \epsilon_o A/(x-x_o-t) \tag{3.2b}$$

where C_{Se} and C_{Air} are the capacitances of the selenium and air capacitors respectively. ϵ_o is the permittivity of free space (a reasonable approximation for air) and ϵ_{Se} is the relative dielectric constant of selenium. x and x_o are the positions of the movable and fixed capacitor plates (Fig. 3.2). t is the thickness of the selenium crystal slab.

Combining the series capacitances, we have:

$$1/C_T = t/\epsilon_{Se}\epsilon_o A + (x-x_o-t)/\epsilon_o A$$

$$= (x-x_o)/\epsilon_o A - t(1-1/\epsilon_{Se})/\epsilon_o A \tag{3.3}$$

where C_T is the total capacitance. $1/C_T$ is a linear function of $(x-x_o)$. If a plot of $1/C_T$ as a function of $(x-x_o)$ is a straight line, this will be a strong argument for the validity of the parallel plate capacitor approximation.

The position x_o is determined by finding the value of x for which $1/C_T = 0$ with no dielectric present ($t = 0$). Rather than decreasing x until the capacitor plates touch, an extrapolation of the plot of $1/C_T$ vs. x to $1/C_T = 0$ gives the value of x_o. This technique prevents damage to the apparatus.

Once x_o is known, a selenium crystal of thickness t is inserted. A new plot of $1/C_T$ vs. x will yield x_1, a new value of x for which $1/C_T = 0$. Thus Eq. (3.3) becomes:

$$0 = (x_1-x_o)/\epsilon_o A - t(1-1/\epsilon_{Se})/\epsilon_o A \tag{3.4}$$

Solving E_2 3.4 for ϵ_{Se}:

$$\epsilon_{Se} = 1/(1 - (x_1-x_o)/t) \tag{3.5}$$

Thus, the dielectric constant can be found from the extrapolated $1/C_T$ vs. x values of x_o and x_1, and the measured thickness of the crystal, t. The area of the capacitor plates, A, and any contribution from fringing fields may be ignored, if the plots of $1/C_T$ vs. x are straight lines.

To accurately determine x_o and x_1, a linear least square fit is made to $1/C_T$ vs. x. However, first a plot of the data is made. Badly scattered points for $1/C_T$ large (very low measured capacitance, less than 5×10^{-15}f) are excluded. Also, measurements yielding $1/C_T$ very small (high measured capacitance, for small values of $(x-x_o-t)$) often deviate from a straight line since the guard ring (see Section 3.3) is relatively ineffective in this region. These, too, are excluded.

The linear least square fit is made in the following manner:

$y(i)$ $i = 1, \ldots, n$	-reciprocal capacitances
$x(i)$ $i = 1, \ldots, n$	-movable capacitor plate positions
n	-number of points
$y = ax+b$	-form of least square fit

$$E(a,b) = \sum_{i=1}^{n} [y(i) - ax(i) - b]^2 \text{ -square error.} \tag{3.6}$$

Minimizing E(a,b) by differentiating with respect to a and b and setting the derivatives equal to zero yields:

$$\frac{\partial E}{\partial a} = 0 \Rightarrow \hat{a} \sum_{i=1}^{n} x(i)^2 + \hat{b} \sum_{i=1}^{n} x(i) = \sum_{i=1}^{n} x(i)y(i) \tag{3.7a}$$

$$\frac{\partial E}{\partial b} = 0 \Rightarrow \hat{a} \sum_{i=1}^{n} x(i) + n\hat{b} = \sum_{i=1}^{n} y(i) \tag{3.7b}$$

where $\hat{a}$ and $\hat{b}$ are the least square values of a and b. For simplicity, define:

$$\sum_{i=1}^{n} y(i) = n\,Y \tag{3.8a}$$

$$\sum_{i=1}^{n} x(i) = n\,X \tag{3.8b}$$

Solving for $\hat{a}$ and $\hat{b}$:

$$\hat{a} = \left[\sum_{i=1}^{n} (y(i) - Y)(x(i) - X) \right] / \sum_{i=1}^{n} (x(i) - X)^2 \tag{3.9a}$$

$$\hat{b} = Y - \hat{a}\,X \tag{3.9b}$$

It is convenient to write the equation of the fitted line as:

$$(y-Y) = \hat{a}\,(x-X) \tag{3.10}$$

which is a point-slope form. The x intercept (y = 0) is given by:

$$x^* = X - Y/\hat{a} \tag{3.11}$$

Replacing $\hat{a}$ by the variable a, the error in x^* is:

$$\Delta x^* = (Y/a^2)\Delta a$$

$$= (y/a)(\Delta a/a) \tag{3.12}$$

Y and a (specifically $\hat{a}$) can be found from Eqs. 3.8a,b and 3.9a. Only Δa (or $\Delta a/a$) must still be determined.

The square error as defined in Eq. (3.6) may now be written:

$$E = \sum_{i=1}^{n} [y(i)-Y -ax(i) + aX]^2 \tag{3.13}$$

Expanding Eq. (3.13), substituting X and Y as defined in Eq. 3.8a,b, and simplifying gives:

$$E = \sum_{i=1}^{n} (y(i)-Y)^2 -2a \sum_{i=1}^{n} (y(i)-Y)(x(i)-X) + a^2 \sum_{i=1}^{n} (x(i)-X)^2 \tag{3.14}$$

Substituting $a = \hat{a} + \Delta a$ and simplifying:

$$E(\hat{a} + \Delta a) = E(\hat{a}) + (\Delta a)^2 \Sigma(x(i)-X)^2 \tag{3.15}$$

where $E(\hat{a})$ is Eq. (3.14) evaluated for $a = \hat{a}$. This error may be expressed as a probability density as a function of the error in slope, Δa:

$$f(\hat{a},\Delta a) = \frac{2}{\pi} \frac{E(\hat{a})}{E(\hat{a}+\Delta a)} = \frac{2}{\pi} \frac{1}{1+\frac{\sum_{i=1}^{n} (x(i)-X)^2}{E(\hat{a},0)} (\Delta a)^2} \tag{3.16}$$

for $\Delta a \ll a$

Defining:

$$K^2 = E(\hat{a},0)/\hat{a}^2 \sum_{i=1}^{n} (x(i)-X)^2 \tag{3.17}$$

The density function $f(K\Delta a/a)$ and a probability distribution function $F(K\Delta a/a)$ may be written:

$$f(K\Delta a/a) = \frac{2}{\pi} \frac{1}{1 + (K\frac{\Delta a}{a})^2} \tag{3.18a}$$

$$F(K\Delta a/a) = \frac{2}{\pi} \tan^{-1} (K\frac{\Delta a}{a}) \tag{3.18b}$$

where $1 >> \Delta a/a \geq 0$. The distribution function F $(K\Delta a/a)$ is defined:

$$F(K\Delta a/a) = \int_{-K\Delta a/a}^{K\Delta a/a} f(z)dz \tag{3.19}$$

This is a form of the Cauchy probability distribution[3.9].

Fig. 3.3 contains two plots:

a. f as a function of $(K\Delta a/a)$

b. F as a function of $(K\Delta a/a)$

To verify that this error analysis is valid for experimental data, a linear least square fit must be made, and E $(\hat{a} + \Delta a)$ computed as a function of $\Delta a/a$. This may be done by evaluating Eq. 3.13:

$$E = \sum_{i=1}^{n} [y(i) - Y - ax(i) + aX]^2$$

for $a = \hat{a} + \Delta a$, where Δa varies from approximately $.9\hat{a}$ to $1.1\hat{a}$. If the Cauchy distribution F adequately describes the square error E as a function of Δa, then a plot of $[E(\hat{a} + \Delta a)/E(\hat{a}) - 1]^{1/2}$ vs. $\frac{\Delta a}{a}$ should be a straight line. This can be seen by substituting the definition of K^2 (Eq. 3.17) into the expression for E in Eq. (3.15) and solving for the function mentioned above:

$$[E(\hat{a} + \Delta a)/E(\hat{a}) - 1]^{1/2} = K\ \Delta a/a \tag{3.20}$$

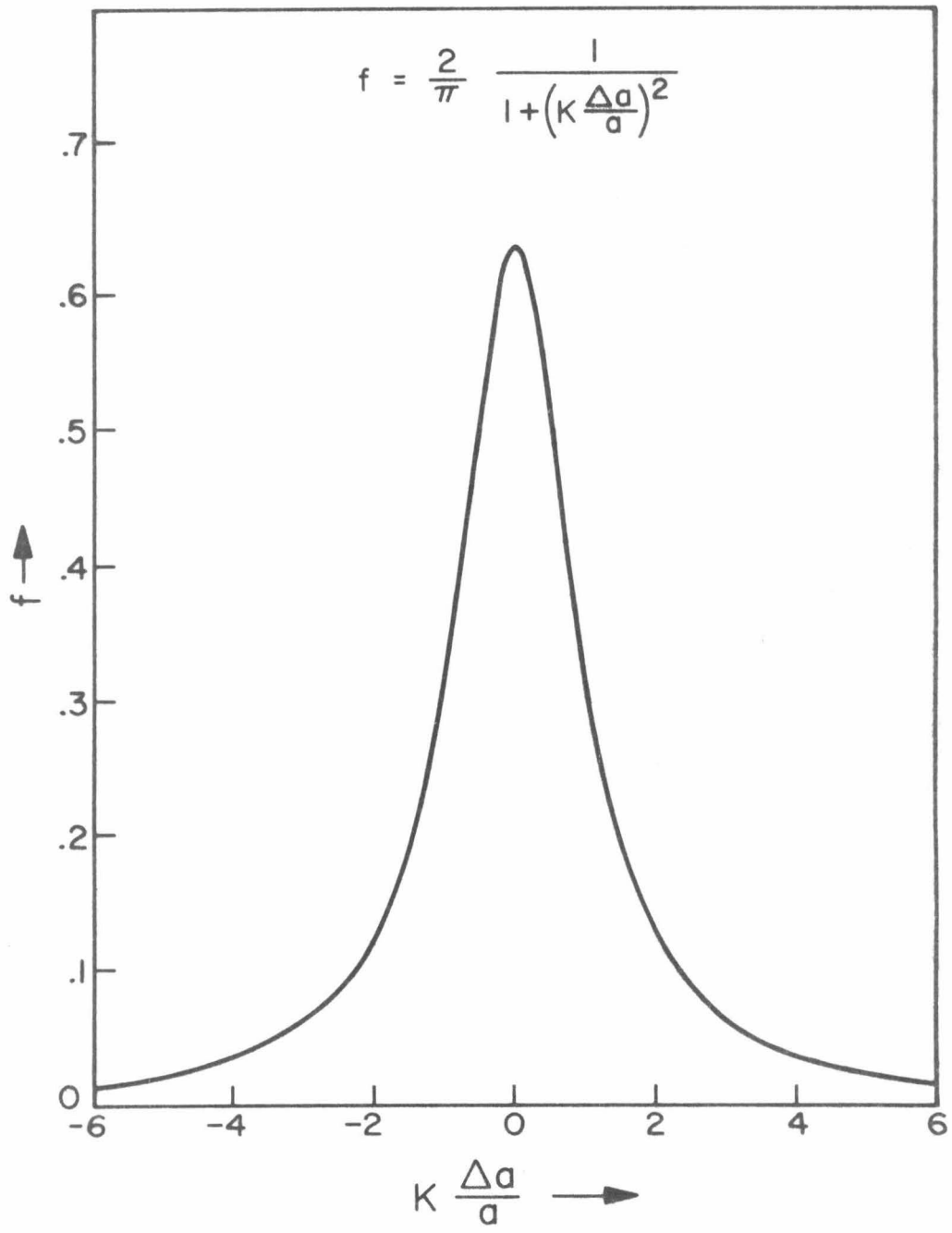

Figure 3.3a A plot of the Cauchy density function f vs. the random variable K $\Delta a/a$.

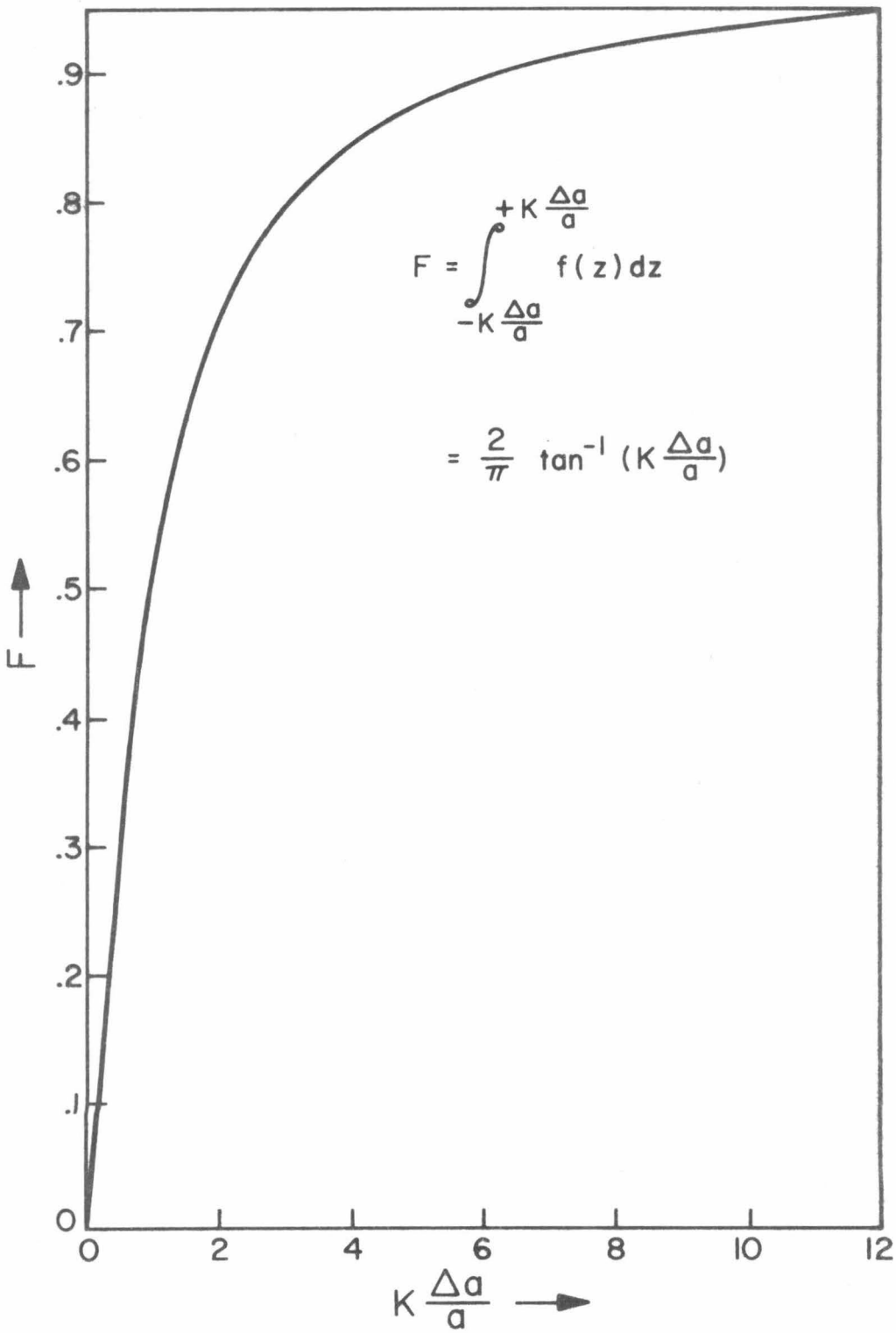

Figure 3.3b A plot of the Cauchy distribution function F vs. the random variable $K\,\Delta a/a$.

If the plot is a straight line, the error analysis is valid, and the slope of the line will give the value of K. Several cases have been plotted in Fig. 3.4.

To determine $(\Delta a/a)$, a confidence level must be chosen; that is, what is the probability that the slope is contained within the interval $(\hat{a}-\Delta a)$ to $(\hat{a} + \Delta a)$? For example, if a 50% confidence level is desired, find what value of $K\Delta a/a$ gives a value of .50 for F in Fig. 3.2b. Then, by knowing K from the method described above, this gives a value of $\Delta a/a$ to be substituted into Eq. (3.12) to obtain Δx^*.

To figure total error, differentiate the expression for the dielectric constant ϵ_{Se} (Eq. 3.5):

$$\Delta\epsilon_{Se} = \left|\frac{\partial\epsilon}{\partial x_1}\right| \Delta x_1 + \left|\frac{\partial\epsilon}{\partial x_o}\right| \Delta x_o + \left|\frac{\partial\epsilon}{\partial t}\right| \Delta t \qquad (3.21a)$$

$$= \epsilon_{Se}^2\left[\left(\frac{\Delta x_1}{t}\right) + \left(\frac{\Delta x_o}{t}\right) + \frac{x_1-x_o}{t}\left(\frac{\Delta t}{t}\right)\right] \qquad (3.21b)$$

The errors $\frac{\Delta x_1}{t}$, $\frac{\Delta x_o}{t}$, $\frac{\Delta t}{t}$ must be kept small since they are multiplied by ϵ_{Se}^2, which is between 10 and 100 for α-monoclinic selenium.

Each determination will yield $\epsilon_i + \Delta\epsilon_i$, where ϵ_i is given by Eq. (3.5) and $\Delta\epsilon_i$ is given by Eq. (3.20). The i refers to the number of the measurement. The resultant value and error are given by:

$$\epsilon_{Se} = \frac{\sum_{i=1}^{m} \epsilon_i/(\Delta\epsilon_i)^2}{\sum_{i=1}^{m} 1/(\Delta\epsilon_i)^2} \qquad (3.22a)$$

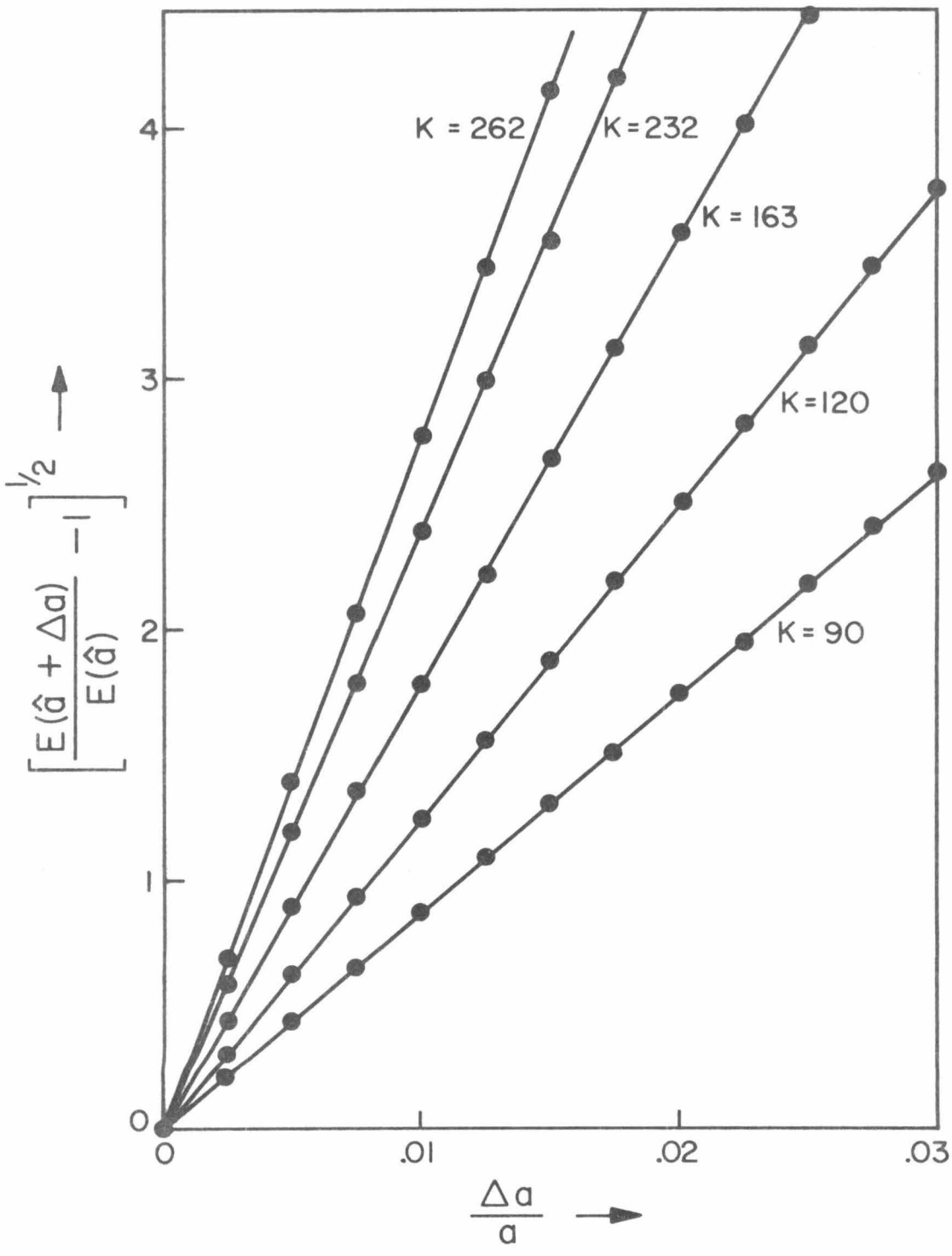

Figure 3.4 A plot to test the validity of using the Cauchy distribution for errors in the linear least square fit.

$$\Delta\epsilon_{Se} = \left[\sum_{i=1}^{m} 1/(\Delta\epsilon_i)^2\right]^{-1/2} \tag{3.22b}$$

The ϵ_i values are weighted according to their respective accuracies[3.10].

3.2.2 Dielectric Anisotropy Model

The low symmetry of α-monoclinic selenium indicates the dielectric constant may be anisotropic (Since the non-orthogonal axes are only 46' from being perpendicular[3.12], all calculations will be made on the basis of α-monoclinic selenium being orthorhombic.). To fully describe the dielectric constant, a second rank tensor is required. Both the dielectric constant and susceptibility tensors, $\underline{\underline{\epsilon}}$ and $\underline{\underline{\chi}}$, will be used in the model.

The polarization $\underline{P}$ is related to the electric field $\underline{E}$ by:

$$\underline{P} = \epsilon_o \underline{\underline{\chi}}\, \underline{E} \tag{3.23}$$

The electric displacement $\underline{D}$ relates $\underline{\underline{\chi}}$ and $\underline{\underline{\epsilon}}$:

$$\underline{D} = \underline{P} + \epsilon_o \underline{E} = \epsilon_o \underline{\underline{\epsilon}} \cdot \underline{E} \tag{3.24}$$

Substituting Eq. (3.23) into Eq. (3.24):

$$\epsilon_o \underline{\underline{\epsilon}} \cdot \underline{E} = \epsilon_o (\underline{\underline{I}} + \underline{\underline{\chi}}) \cdot \underline{E} \tag{3.25a}$$

$$\epsilon_E = (\underline{\underline{\epsilon}} \cdot \underline{E}) \cdot \underline{E}/\underline{E} \cdot \underline{E} \tag{3.25b}$$

$$\epsilon_E = 1 + (\underline{\underline{\chi}} \cdot \underline{E} \cdot \underline{E})/\underline{E} \cdot \underline{E} \tag{3.25c}$$

$$\epsilon_E = 1 + \chi_E \tag{3.25d}$$

where $\underline{\underline{I}}$ is the unit diagonal tensor:

$$\underline{\underline{I}} = \begin{pmatrix} 1 & 0 & 0 \\ 0 & 1 & 0 \\ 0 & 0 & 1 \end{pmatrix} \tag{3.26}$$

and ϵ_E is the relative dielectric constant along the direction of the electric field $\underline{E}$. The tensors $\underline{\underline{\epsilon}}$ and $\underline{\underline{\chi}}$ for orthorhombic crystals are diagonal[3.11]:

$$\underline{\underline{\epsilon}} = \begin{pmatrix} \epsilon_a & 0 & 0 \\ 0 & \epsilon_b & 0 \\ 0 & 0 & \epsilon_c \end{pmatrix} \tag{3.27a}$$

$$\underline{\underline{\chi}} = \begin{pmatrix} \chi_a & 0 & 0 \\ 0 & \chi_b & 0 \\ 0 & 0 & \chi_c \end{pmatrix} \tag{3.27b}$$

when a, b and c are the orthogonal crystal axis directions. The elements along the diagonal in general are independent. However, in orthorhombic sulfur and α-monoclinic selenium, they may be simply related.

Both materials consist of 8-atom rings. Assuming the rings to be planar (which they are not), the molecular susceptibility tensor $\underline{\underline{\beta}}$ of a ring can be written:

$$\underline{\underline{\beta}} = \begin{pmatrix} \beta_1 & 0 & 0 \\ 0 & \beta_2 & 0 \\ 0 & 0 & \beta_1 \end{pmatrix} \tag{3.28}$$

where the b direction is taken normal to the ring. β_1 and β_2 are the susceptibilities (or polarizabilities) in and perpendicular to the

'plane' of the ring. In orthorhombic sulfur there are two orientations of rings. $\underline{\underline{\beta}}$'s for these two orientations of rings can be found by rotating[3.12] the tensor in Eq. (3.26) and averaging the two new tensors, since susceptibility tensors are additive. The average plane normals of the two classes of rings are inclined $\pm 51.4^{o}$ with respect to the b axis, the normals being in the a-b plane (calculated from Ref. 3.13). This gives a susceptibility tensor of:

$$\underline{\underline{\chi}} = \begin{pmatrix} .389\beta_1 + .611\beta_2 & 0 & 0 \\ 0 & .611\beta_1 + .389\beta_2 & 0 \\ 0 & 0 & \beta_1 \end{pmatrix} \tag{3.29}$$

Thus, from Eqs. 3.25d and 3.29:

$$\begin{aligned} \epsilon_a &= 1 + .389\beta_1 + .611\beta_2 \\ \epsilon_b &= 1 + .611\beta_1 + .389B_2 \\ \epsilon_c &= 1 + \beta_1 \end{aligned} \tag{3.30}$$

The dielectric constants of sulfur have been measured[3.8]:

$$\epsilon_a = 3.75 \tag{3.31a}$$

$$\epsilon_b = 3.95 \tag{3.31b}$$

$$\epsilon_c = 4.44 \tag{3.31c}$$

Solving for β_1 directly, and for β_2 from both the a and b *equations*, we

have:

$$\beta_1 = 3.44 \tag{3.32a}$$

$$\beta_2 = 2.18 \quad , \quad 2.30 \tag{3.32b}$$

The two values for β_2 are quite close, being about 5% apart. So, to within 5% in susceptibility, the S_8 rings in orthorhombic sulfur can be considered planar, with the susceptibility (and dielectric constant) characterized by 2 parameters:

1. β_1, the susceptibility in the plane of the ring.
2. β_2, the susceptibility normal to the plane of the ring.

The extension to α-monoclinic selenium is obvious. There are again two orientations of rings over which to average the rotated susceptibility tensors (Eq. 3.26). The rotations are slightly more complicated, since rotations about 2 axes are required for each ring. The important difference is that the angle between the b axis and all plane normals is 23.5° instead of 51.4° (calculated from Ref. 3.14). The $\underline{\underline{\chi}}$ tensor is given by:

$$\underline{\underline{\chi}} = \begin{pmatrix} .983\beta_1 + .017\beta_2 & 0 & 0 \\ 0 & .159\beta_1 + .841\beta_2 & 0 \\ 0 & 0 & .856\beta_1 + .144\beta_2 \end{pmatrix} \tag{3.33}$$

From Eqs. 3.25d and 3.33:

$$\epsilon_a = 1 + .983\beta_1 + .017\beta_2 \tag{3.34a}$$

$$\epsilon_b = 1 + .159\beta_1 + .841\beta_2 \tag{3.34b}$$

$$\epsilon_c = 1 + .856B_1 + .144\beta_2 \tag{3.34c}$$

where the letter subscripts refer to the a, b, and c crystal axes. Three non-coplanar measurements of the dielectric constant are needed to test the validity of the model for α-monoclinic selenium.

3.3 Experimental Apparatus

The apparatus was designed to determine a dielectric constant from capacitance measurements and measured physical parameters. The capacitance measurements were made using a Boonton Electronics Corporation Direct Capacitance Bridge, Model 75C. It is a variable frequency (5-500 kc) bridge, accurate to better than 2% in the range 0 - .05 pf, and to better than 0.25% in the range .05 - 1.0 pf.

The specific design of the apparatus for the dielectric constant measurement was guided by the four constraints discussed in Section 3.2:

1. The crystals must be free of voids.
2. Errors imposed by geometry must be carefully considered.
3. Intimate electrical contact to the crystals is impossible.
4. The crystals are very fragile.

Constraint 1. imposes a limit on the size of the crystals which can be used. Since sufficiently many crystals were available in the 1-1 1/2mm range, the apparatus was designed for a 1mm crystal. Constraint 2. suggests a guard ring structure, probably with a circular

electrode and an annular guard ring. This would maintain a uniform electric field region over the crystal face in the vicinity of the upper electrode. Constraints 3. and 4. suggest the crystal be physically placed between two electrodes, and an air layer be allowed for between the crystal and one capacitor plate. Rather than trying to minimize this, a movable electrode to vary the air layer thickness was decided upon.

Fig. 3.1 shows the essential features of the apparatus. The device is cylindrically symmetric about the vertical axis. The upper electrode diameter was made .020" (1/2 mm), somewhat smaller than the usable size of the crystals. The lower electrode is larger, since the separate guard ring structure need only be at one electrode (in this case, the upper one). The lower electrode is embedded in a 1/4" diameter teflon rod for electrical insulation, physical support, and ease of fabrication. The side of the teflon cylinder is coated with aluminum (by vacuum evaporation) for electrical shielding. The upper electrode structure is essentially a guard ring, with a small hole for a .020" aluminum wire, insulated from the brass guard ring electrode by a thin (~ .001") insulating layer of epoxy. The structure will act as a guard ring as long as the electrode guard ring spacing (~ .001") is small compared to the air layer thickness.

The upper electrode structure is attached to a micrometer to provide accurate vertical position, to accommodate various thickness crystals, and to separate the electrodes for easy access. The electrodes are enclosed within a loosely fitting aluminum shield which provides

further shielding and support, but which can be easily removed for access.

The electrodes are connected to the capacitance bridge through the center conductors of two short co-axial lines. The outer conductor of both lines lead from the shield of the apparatus to the ground terminal of the bridge. The bridge circuit and test apparatus electrical connections appear in Fig. 3.5. The transformer provides voltages across AC and CB equal in amplitude and phase. Then, if the capacitances between AD and DB are equal, the detector input voltage across CD is zero. At the null, C and D are at the same potential, C supplying the guard ring potential mentioned earlier. The conductance portion of the bridge is not shown, since no measurable conductance was observed.

For capacitance measurement, the upper electrode is disconnected, and the bridge set to zero capacitance at the detector null. After reconnecting the upper electrode, the actual capacitance at null is measured. After a series of measurements as a function of micrometer position are taken, the zero is rechecked by disconnecting the upper electrode. If the zero has shifted slightly, a linear correction is applied to the measured values (If the zero has shifted by C_o, the correction applied to the $m^{\underline{th}}$ measurement is $\frac{m}{n+1} C_o$, where n was the number of measurements.). This assumes a linear drift rate. If C_o is large, the measurements are retaken.

The apparatus was tested with a slab of quartz with a dielectric

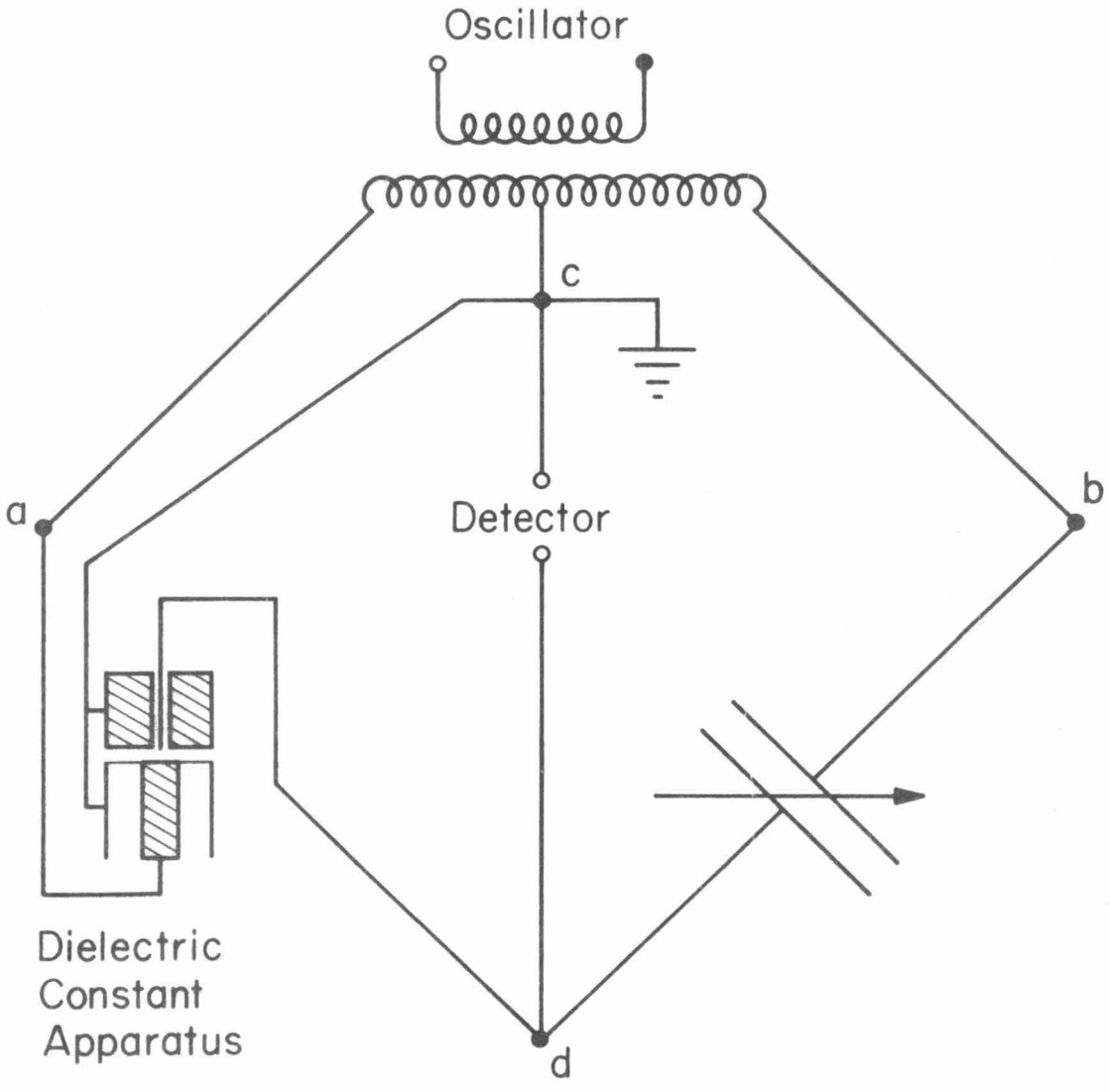

Figure 3.5 The capacitance bridge and its connections to the dielectric constant measurement apparatus.

constant 4.3[3.14]*. The experimentally determined value was 4.19 ± .20, sufficiently close to 4.3.

The crystal to be measured is oriented and mounted on a flat metal block with black wax (de Khotinsky cement). To prevent damage to the crystal by heating, the wax is softened with toluene, and then allowed to harden. The crystal is then polished on a polishing cloth with a slurry of 1.0μ alumina powder in distilled water. After measurement of capacitance, the thickness is measured (on a Carson-Dice Electronic Micrometer). If further measurements on the same crystal are to be made, it is rewaxed to the metal block and repolished.

3.4 Results

The dielectric constant was measured for three crystal orientations:

1. Along the [101] direction
2. As near as possible to the [010] direction
3. Another non-coplanar direction.

The first was an obvious choice, since the (101) face is the best developed and most easily recognized face on the crystals[3.6]. The second was chosen for two reasons: the [010] direction is parallel to the two-fold rotation axis, the only "natural" direction in the crystal; along this direction, the rings are viewed nearly normal to the plane

---

*Actually, the dielectric constant of quartz is mildly anisotropic, with values of 4.27 and 4.34. Since they are quite close, and the orientation of the slab was unknown, the value of 4.3 was chosen for testing the apparatus.

of the rings. The third was needed to check the two parameter model of Section 3.2.1.

The error evaluation (Section 3.2.1) was done with a confidence level of 0.68, corresponding to one standard deviation in the normal probability distribution.

The approximate crystal directions, the actual crystal plane unit normal vectors, and the experimentally determined dielectric constants are found in Table 3.2. (Also see Fig. 3.6.) The large error in the [111] measurement is unfortunate. However, the problem comes from the $\epsilon_{Se}^{\ 2}$ factor in Eq. 3.21b. Small errors in the intercepts x_o and x_1, and the thickness t have a large effect upon the dielectric constant error. In the case of the individual [111] measurements, the Δx_1 term was consistently larger than in the case of the [101] and [010] measurements. Because of the $\epsilon_{Se}^{\ 2}$ factor, this method is unusable for materials with a dielectric constant greater than 10.

The ring susceptibilities calculated from the [101] and [010] direction values are:

$$\begin{aligned} \beta_1 &= (7.98 \pm .34) \\ \beta_2 &= (4.70 \pm .52) \end{aligned} \tag{3.35}$$

Using β_1 and β_2, the calculated value for the [111] entry of Table 3.2 is 8.09 ± .39, compared to 7.73 ± .87. The difference between the calculated and experimental values, .36 is well within the ± .87 error of the experimental determination. Again using β_1 and β_2, the calculated

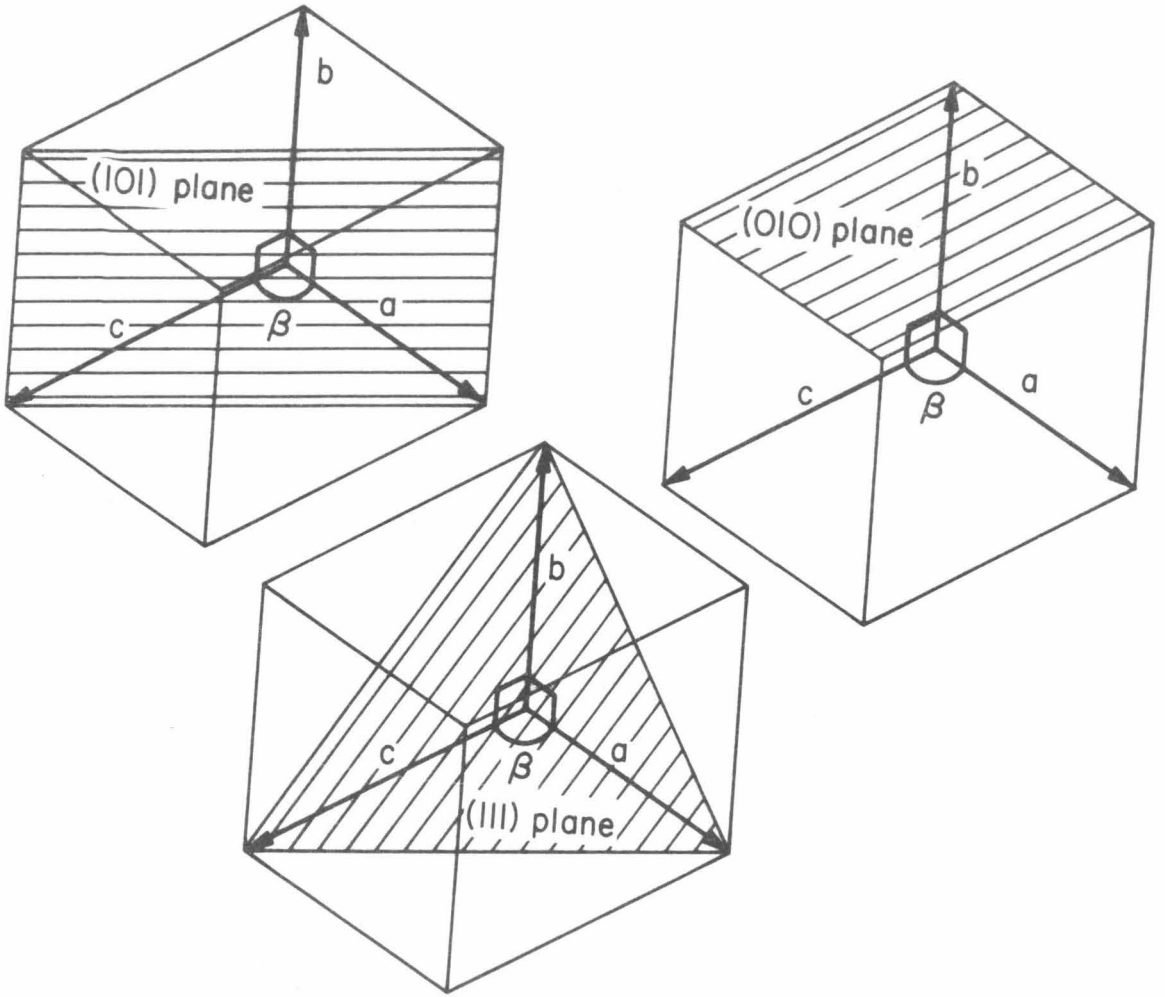

Figure 3.6abc The (101), (010), and (111) planes in the α-monoclinic selenium unit cell; a, b and c respectively.

TABLE 3.2

MEASURED DIELECTRIC CONSTANT

ANISOTROPY IN α-MONOCLINIC SELENIUM

Approximate Crystal Direction	Unit Normal Vector	Dielectric Constant
[101]	(.789, .000, .615)	8.73 ± .25
[010]	(.211, .976, .058)	6.06 ± .38
[111]	(.526, .515, .676)	7.73 ± .87

dielectric constants along the three crystal axes are given in Table 3.3. The corresponding values calculated directly from the results in Table 3.2 would not be meaningful, because of the large error in the [111] value. To do this correctly, measurements should be made along the three crystal axis directions (or at least along 3 mutually orthogonal directions).

3.5 Discussion

The two parameter dielectric anisotropy model characterizes orthorhombic sulfur quite well. For physical insight, however, the dielectric constant values should be considered with the molecular pictures[3.16] of Fig. 3.7a, b, c, d. The unit cell for the sulfur is shown in Fig. 3.7d. The lattice parameters[3.17] are:

$a = 10.4646 \pm .0001A$

$b = 12.8660 \pm .0001A$

$c = 24.4860 \pm .0003A$

Figures 3.7a, b and c are projections down the a, b and c axes respectively. The a and b projections look 'down the throat' of the rings, and have lower dielectric constants (3.75, 3.95) than the c projection, which looks at the rings on edge and has the highest dielectric constant (4.44). This indicates the susceptibility in the plane of the rings (β_1) should be greater than the susceptibility normal to the rings (β_2). The model confirms this (Eq. 3.32a,b):

$\beta_1 = 3.44$

$\beta_2 = 2.24$

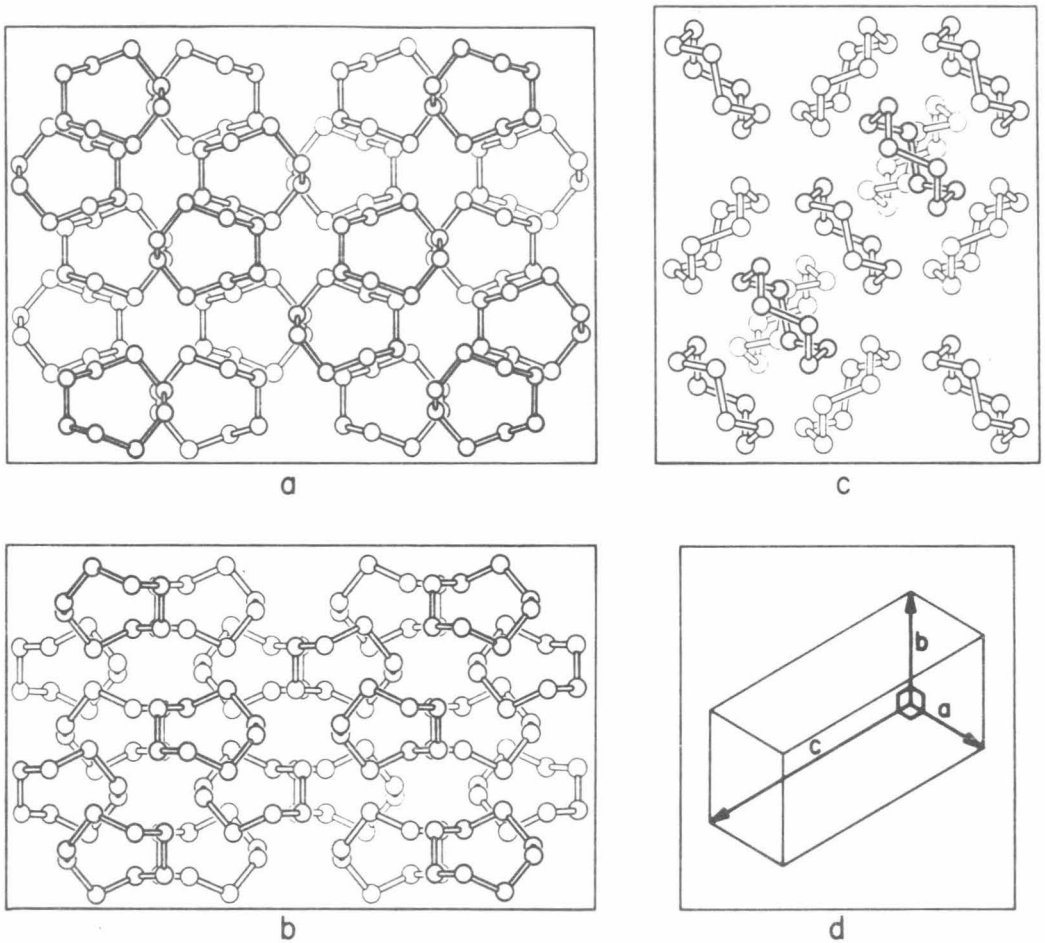

Figure 3.7abcd Orthorhombic sulfur. a, b and c are the projections of the S_8 ring molecules along the a, b and c crystal axes respectively. d is the unit cell for orthorhombic sulfur.

TABLE 3.3

DIELECTRIC CONSTANTS OF α-MONOCLINIC SELENIUM ALONG THE CRYSTAL AXES

Crystal Direction	Axis Name[3.15]	Calculated Dielectric Constant
[100]	a	8.93 ± .34
[010]	b	6.02 ± .49
[001]	c	8.52 ± .36

The three crystal axis projections for α-monoclinic selenium are shown in Fig. 3.8a, b, c. If the model is valid for the selenium, ε_a should be the largest, ε_c intermediate but close to ε_a, and ε_b should be the smallest. This is born out semi-quantitatively by the measured values:

1. The [101] value of 8.73 is the largest measured. The dielectric constant along this direction is a linear combination of the [100] and [001] susceptibilities, predicted larger than the [010] value.
2. The [010] value of 6.06 is the smallest value measured. It is determined predominently by the ring normal susceptibility, β_2, predicted smaller than the ring plane susceptibility.
3. The [111] value of 7.73 is indeed intermediate, being a linear combination of all three principal axis susceptibilities.

Quantitatively, the validity of the model is somewhat in question. The [111] value is significantly different from the value predicted, using the two parameter model and the [101] and [010] values determined experimentally. This may be due to the errors in the measurements. Unfortunately, the method used to determine the dielectric constant was not as accurate as one would like. The cause may also be attributed to interactions between the rings, neglected in the model. The selenium valence electrons are less tightly bound than those of sulfur, permitting the electrons to range further from the nucleus. This would indicate the Se_8 rings interact more than the S_8 rings do. Thus, even with a very accurate dielectric constant determination, the model would probably not be as accurate in describing α-monoclinic selenium as it is for orthorhombic sulfur.

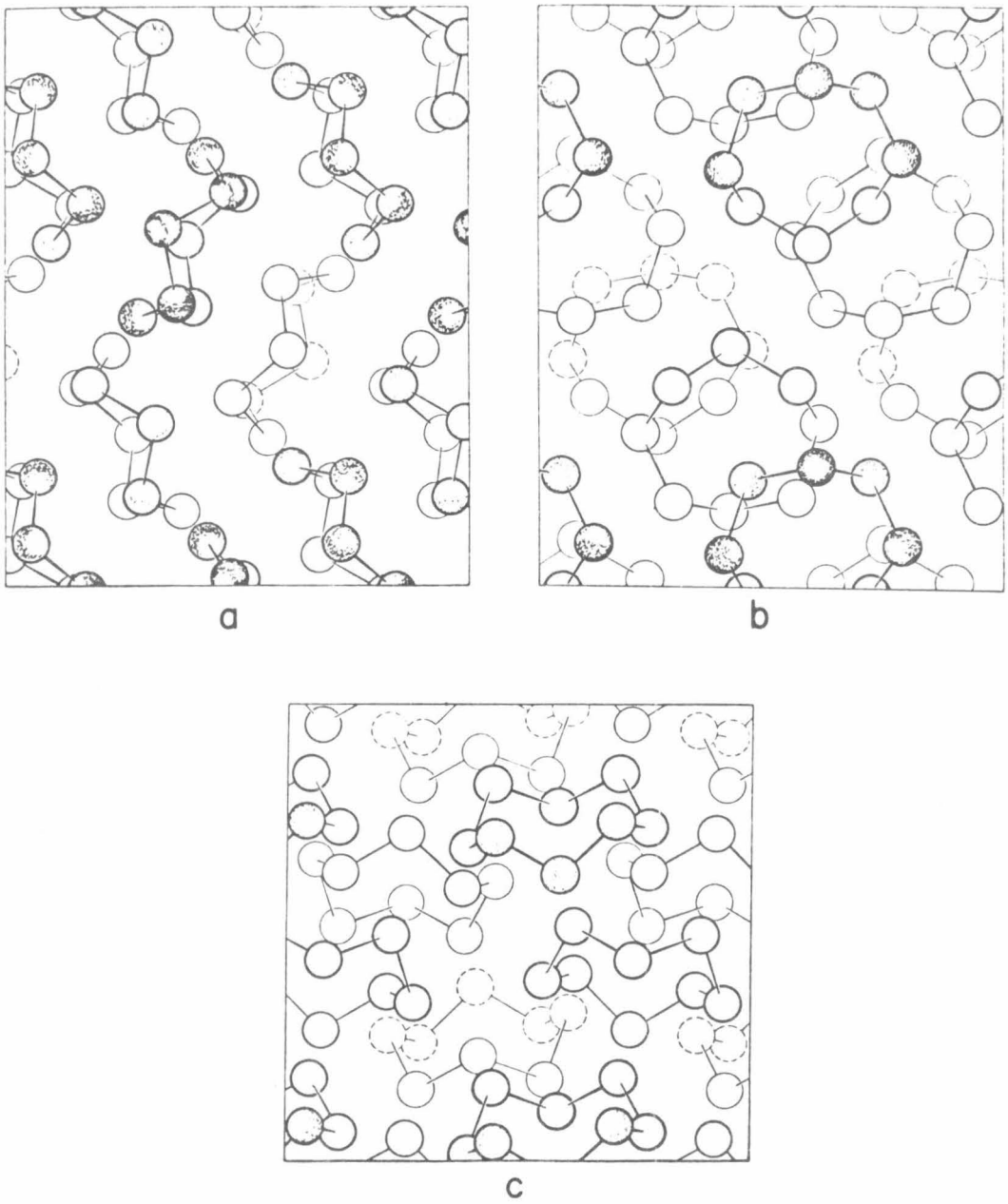

Figure 3.8abc α-monoclinic selenium. a, b and c are the projections of the Se_8 ring molecules along the a, b and c crystal axes respectively.

CHAPTER IV

OPTICAL ABSORPTION

4.1 Introduction

Although optical properties of amorphous and trigonal selenium have been studied extensively[4.1 - 4.4], Prosser[4.5] alone has reported optical measurements on α-monoclinic selenium, and only for a range of photon energy of 1.43 - 2.09 eV. The upper limit was set by high absorption in the vicinity of the crystal absorption edge. While Prosser's sample was large enough (3mm x 3mm) to permit reflection as well as transmission measurements, it was too thick (50μ) to transmit sufficiently in the vicinity of the absorption edge and beyond.

The platelets (Section 1.1.2 and Fig. 1.3) grown by evaporation of a selenium saturated CS_2 solution are ideal for extending transmission measurements. Assuming a simple form for absorption, the transmitted intensity (for no reflection) is given by:

$$T = I\, e^{-\alpha(h\nu)d} \tag{4.1}$$

whose T and I are the transmitted and incident intensities, respectively, $\alpha(h\nu)$ is the absorption coefficient at the energy $h\nu$ and d is the thickness of the absorbing material. Platelets 0.5μ thick would allow determination of $\alpha(h\nu)$ 100 times as large as Prosser's, since his crystals were 100 times thicker. For a platelet 0.07μ thick (the thinnest one measured), an absorption coefficient over 700 times Prosser's could be reached.

The disadvantage of the platelets is their size. Only several hundred microns across, they are too small to permit reflection measurements. Also, they have to be grown on a substrate, and cannot be removed and repositioned without damage.

There has been one other optical measurement on allegedly α-monoclinic selenium. Fergusson[4.8] has reported measuring the absorption coefficient of "α-monoclinic selenium in carbon disulfide" for photon energies in the range 2.88 - 3.49 eV. The absorption coefficient is reported to have a peak at about 3.22 eV. This is interesting from the photon energy alone, since 2.88 - 3.49 eV is much higher than 2.09 eV where Prosser's work was terminated.

It was decided to extend Prosser's absorption measurements to higher energies using thin platelets, and to measure absorption of selenium in solution, to compare the results. It was also decided to measure absorption at low temperatures, since there was qualitative evidence of an absorption edge shift in α-monoclinic selenium. (Section 4.2.3).

4.2 Experimental Apparatus and Sample Preparation

Section 4.2.1 describes the measurement of transmission through platelets at room temperature. Section 4.2.2 describes the measurement of transmission through selenium in several solvents, from which α-monoclinic crystals have been grown (CS_2, trichlorethylene and toluene). Section 4.2.3 describes measurement of transmission through platelets at low temperatures (approximately $80^{o}K$ and $10^{o}K$).

4.2.1 Platelets at Room Temperature

The experimental setup is shown in Fig. 4.1. Two different light sources were used, a Sylvania DXM Tungsten Halogen Lamp, and a PEK X75 Xenon Lamp. The first was used below about 3 eV, the second, for all higher energy measurements. M1 is a spherical mirror used to focus the image of the light source on the input slit. The monochromator used was a Spex Model 1400-11 3/4 Meter Czerny-Turner Spectrometer, a double monochromator equipped with two 600 line/mm gratings blazed at 5000 A. A mechanical chopper was used at the monochromator input.

The monochromatic light at the output was focussed by a 90^{o}, off-axis, paraboloid, 6:1 reducing mirror (M2). The light passed through the sample and was detected by a vacuum photodiode. Because the monochromator employs gratings, precautions had to be taken to reject non-first order light. This was done by choosing photodiodes with sensitivities over about an octave in energy. Three different ones were used:

1. RCA 917, with an S-1 photocathode, used from 1.1 to 2.1 eV.
2. Sylvania 929, with an S-4 photocathode, used from 1.9 to 3.5 eV.
3. RCA 935, with an S-5 photocathode, used from 3.1 to 4.6 eV.

The preamplifier was a home-built model with amplifications of 10, 100, and 1000. The preamplifier drove a PAR HR-8 Lock-In Amplifier, which received a 45 c/s lock-in signal from the chopper. The output of the lock-in amplifier was read on a Fairchild Model 7050 digital voltmeter. With this system it was relatively easy to cover more than 3 orders of magnitude in relative transmission with good reproducibility

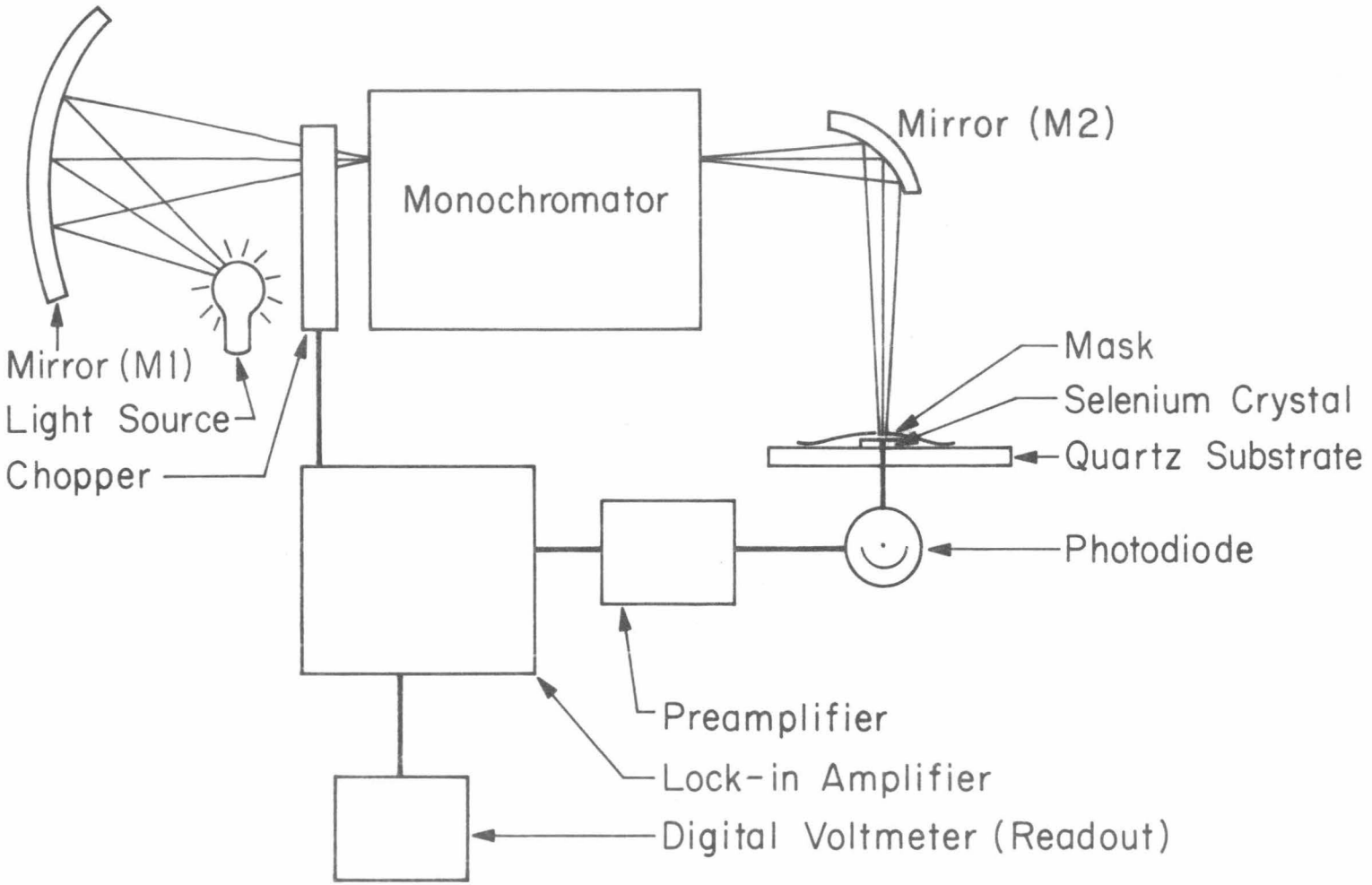

Figure 4.1 Apparatus for room temperature transmission measurements on α-monoclinic selenium platelets.

and little scatter.

The sample was an α-monoclinic selenium platelet (described in Section 1.1.2) grown on a quartz optical window. A mask was made from aluminum foil, in which a small hole had been drilled. The mask was held in place with a mixture of Duco Cement and butyl acetate. Since the butyl acetate has had no visible effect on platelets, the mask can be removed by immersing the sample assembly in the solvent. Masks with holes of 100μ, 150μ, 170μ and 200μ were used, depending on the size of the crystal.

The apparatus was calibrated without the crystal using a mask on a clean quartz window. The response at a given energy was the output signal with the crystal divided by the output signal without the crystal. This ignores reflections, but they are negligible for large absorption. The general problem of transmission, reflection, and absorption is treated in Appendix B.

The thickness of a platelet was determined using an interferometer. The platelet and substrate were overcoated by vacuum evaporation with gold*, then aluminum. To resolve the ambiguity inherent in interferometric measurement of sharp steps, two different wavelengths of light were used: 5351 A line of thallium, and the 5884A sodium D lines. Consistency arguments were used to determine the thickness.

---

*The aluminum provided the reflecting surface, but selenium reacts with that metal. A thin gold layer was applied first as a buffer.

4.2.2 Solutions

Transmission measurements were made on solutions using a Cary Model 14 Spectrophotometer, which uses a dual beam and a time sharing system to eliminate the effect of the solvent and container. To check this, the transmission cells were always filled with unadulterated samples of the solvent to be employed and a transmission spectrum was taken before the solution was placed in the cell.

Transmission measurements were made of 99·99 per cent pure selenium dissolved in CS_2, in trichlorethylene (TCE) and in toluene. The CS_2 used was reagent grade. The TCE was reagent grade which was subsequently distilled prior to use. The toluene was spectroscopic grade.

The solutions were prepared by allowing a fine powder of amorphous selenium to dissolve in approximately one liter of solvent at room temperature. After one week, the solutions were diluted by about 10% (to make them sufficiently undersaturated that a small amount of evaporation would not cause any precipitation). Next, they were filtered twice through a fritted glass filter funnel to remove the undissolved selenium.

The concentration of each solution was determined by weighing residues from evaporation of a known amount of solvent. Thus, the concentration was the weight of selenium solution residue minus the pure solvent residue divided by the volume of solvent evaporated. The weight of the pure solvent residue was always much smaller than the selenium solution residue ($< 3\%$), except for the toluene, which dis-

solved so little selenium, quantitative measurements of transmission were not made.

4.2.3 Low Temperature Measurements

The low temperature measurements were motivated by a very simple experiment: immersion of a bulky α-monoclinic crystal into liquid nitrogen. At room temperature, the crystal appears dark, with highly reflecting crystal faces. At liquid nitrogen temperature ($77^{o}K$), the crystal appears orange, and the high reflection from the faces is not noticeable.

A Texas Instrument 1/2 Liter Cryoflask was used for the low temperature measurements. The light from the monochromator entered the cryoflask through a quartz window, passed through the hole in the mask, the crystal, and the quartz substrate, and exited the cryoflask through another quartz window. The light then entered a vacuum photodiode. For polarization measurements, a polarizer was inserted between the monochromator and the cryoflask. A 10 cm focal length quartz lens replaced the 6:1 focussing mirror in Fig. 4.1. The remainder of the optics is described in Section 4.2.1. For these measurements, a PAR Model 112 X100 Preamplifier and PAR Model 122 Lock-In Amplifier replaced those mentioned in Section 4.2.1.

The cryoflask was evacuated, and the cold reservoir filled with liquid nitrogen. For liquid helium measurements, the cryoflask was first cooled with liquid nitrogen. When the temperature stabilized, the liquid nitrogen was removed, and replaced by liquid helium. The

temperature near the sample was monitered with a Solitron Germanium Cryogenic Thermometer, very useful in the range 2.2^{o} - 100^{o}K. For the low temperature measurements, rubber cement replaced the Duco Cement in the adhesive.

4.3 Results

The results of room temperature measurements on platelets are given in Section 4.3.1. The results of room temperature solution measurements are given in Section 4.3.2, and are compared with the room temperature platelets results. The low temperature platelets results are given in Section 4.3.3, and are also compared to the room temperature platelets results. Also, the results of polarization measurements are given.

4.3.1 Platelets at Room Temperature

Fig. 4.2 is a semi-log plot (of every second point) of a relative transmission measurement on platelet Se04. The transmission below 2.05 eV is relatively constant, and not shown. It is this constant level which is arbitrarily called 100% transmission (relative transmission = 1.0).

Fig. 4.3 is a plot of -ln(T)/d (see Eq. 4.1) for two samples of different thickness, where T is relative transmission and d the corresponding thickness. Sample Se04 was .4102 ± .0061μ thick while Se09 was .1060 ± .0040μ thick. The errors represent the 95 per cent confidence limits of the Student's t test calculated from repeated measurements. Since the relative transmission was measured, not the

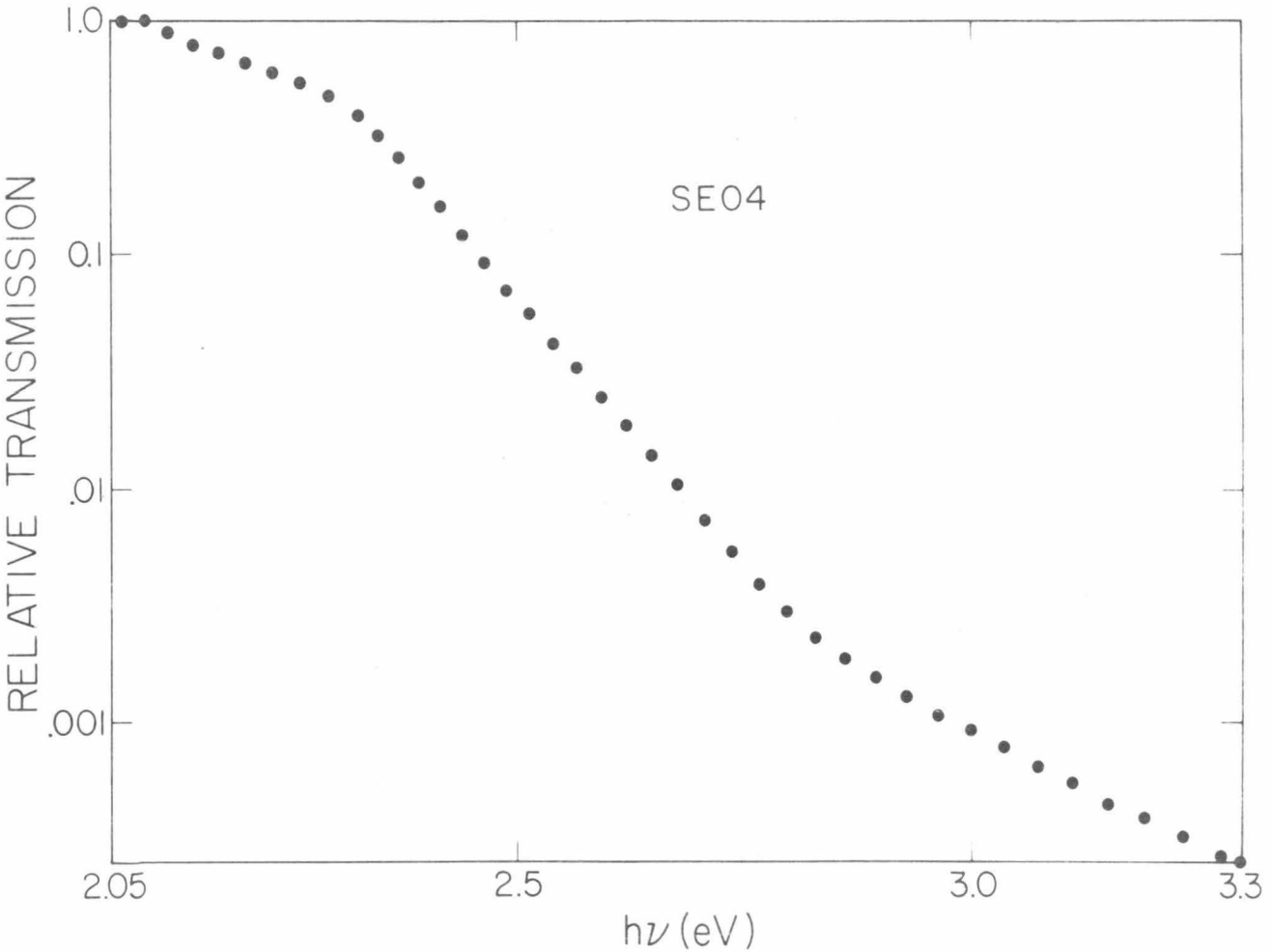

Figure 4.2 Relative transmission of a platelet (Se04) of α-monoclinic selenium.

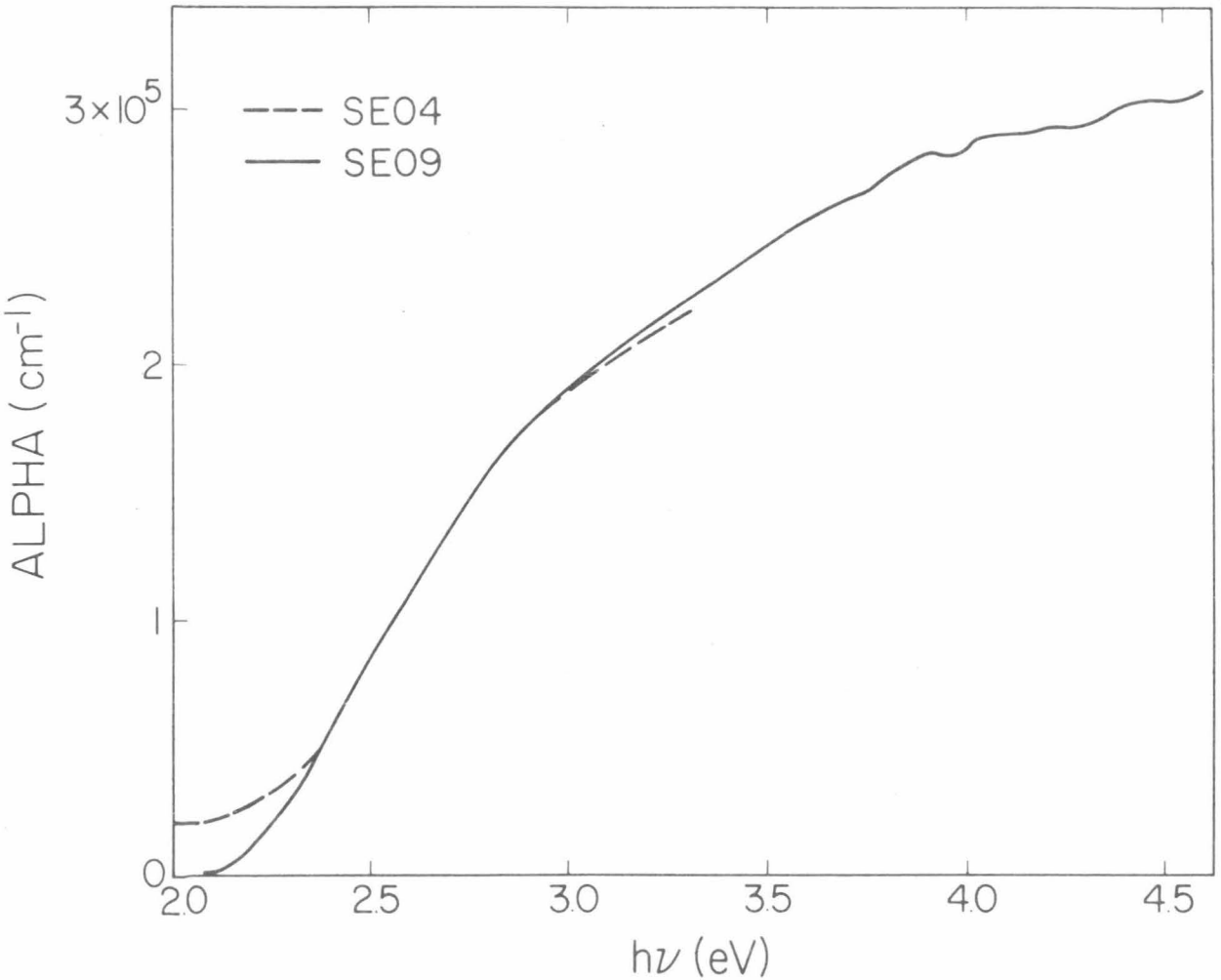

Figure 4.3 Absorption coefficient of α-monoclinic selenium. Actually, -ln (transmission)/ thickness plotted for two platelets, corrected vertically for reflection.

absolute transmission, the highest transmission point of Se09 was set at unity and the level of Se04 was chosen to fit the two curves in the region of high absorption where reflections are unimportant. A calculation of the expected transmission (see Appendix B) was made for Se09, using the thickness and Prosser's data:

$n = 2.74$ $k \simeq 0$	at $\lambda = .592\mu$ (2.09 eV)
$n_o \simeq 1$	refractive index of air
$n_2 = 1.544$	refractive index of quartz
$a = 0.1060\mu$	platelet thickness

The expected transmission was 0.99. Because of the thickness, wavelength of light, and the index of refraction, the transmission is very near a peak, a maximum in the transmission channel spectrum. This can be shown by evaluating Eq. B.6 for thicknesses near 0.1060μ. 0.99 is close enough to unity to justify the choice of $\alpha = 0$. The calculation for Se04 ($a = .4102\mu$) gives 0.78, in good agreement with the actual position of the Se04 curve.

The plot of α in Fig. 4.3 shows a tail between 2.0 and 2.35 eV, a linear region from 2.35 to 2.85 eV, another linear region from 2.85 to 3.7 eV, and a rather sloppy region due to low light level above 3.7 eV. Despite the scatter, the average slope above 3.7 eV is definitely smaller than below 3.7 eV. An extrapolation of the linear region (from 2.35 to 2.85 eV) to $\alpha = 0$ gives an absorption edge of about 2.20 eV.

4.3.2 Solutions at Room Temperature

The results of transmission measurements through solutions containing selenium are plotted in Fig. 4.4. The atomic extinction coefficient is plotted, since the molecular species present in solution is not known. The coefficient is defined:

$$T = I\ 10^{-\gamma(h\nu)cd} \tag{4.2}$$

where T and I are the transmitted and incident intersities (neglecting reflections), $\gamma(h\nu)$ is the atomic extinction coefficient (liters per gram mole centimeter), c is the concentration of the solute in the solvent (gram moles per liter), and d is the length of the light path through the solution (centimeters). $\gamma(h\nu)$ is related to α (Eq. 4.1) by:

$$\gamma(h\nu) = \alpha(h\nu)/c\ \ln(10) \tag{4.3}$$

where ln(10) is the natural logarithm of 10.

Results using CS_2 and trichlorethylene (TCE) are plotted. Since very little absorption was found using toluene, the results are not shown. The amount of selenium dissolved by the toluene was very small, indicating there was insufficient selenium in solution to absorb appreciably. However, α-monoclinic platelets were grown using all three solutions, indicating the solvents act similarly upon the selenium*.

---

*Not all solvents will do this. Kolb[4.6] has reported growing trigonal selenium crystals from an aqueous Na_2S solution. Iizima[4.7] has used a methyl alcohol solution of Na_2S with similar results.

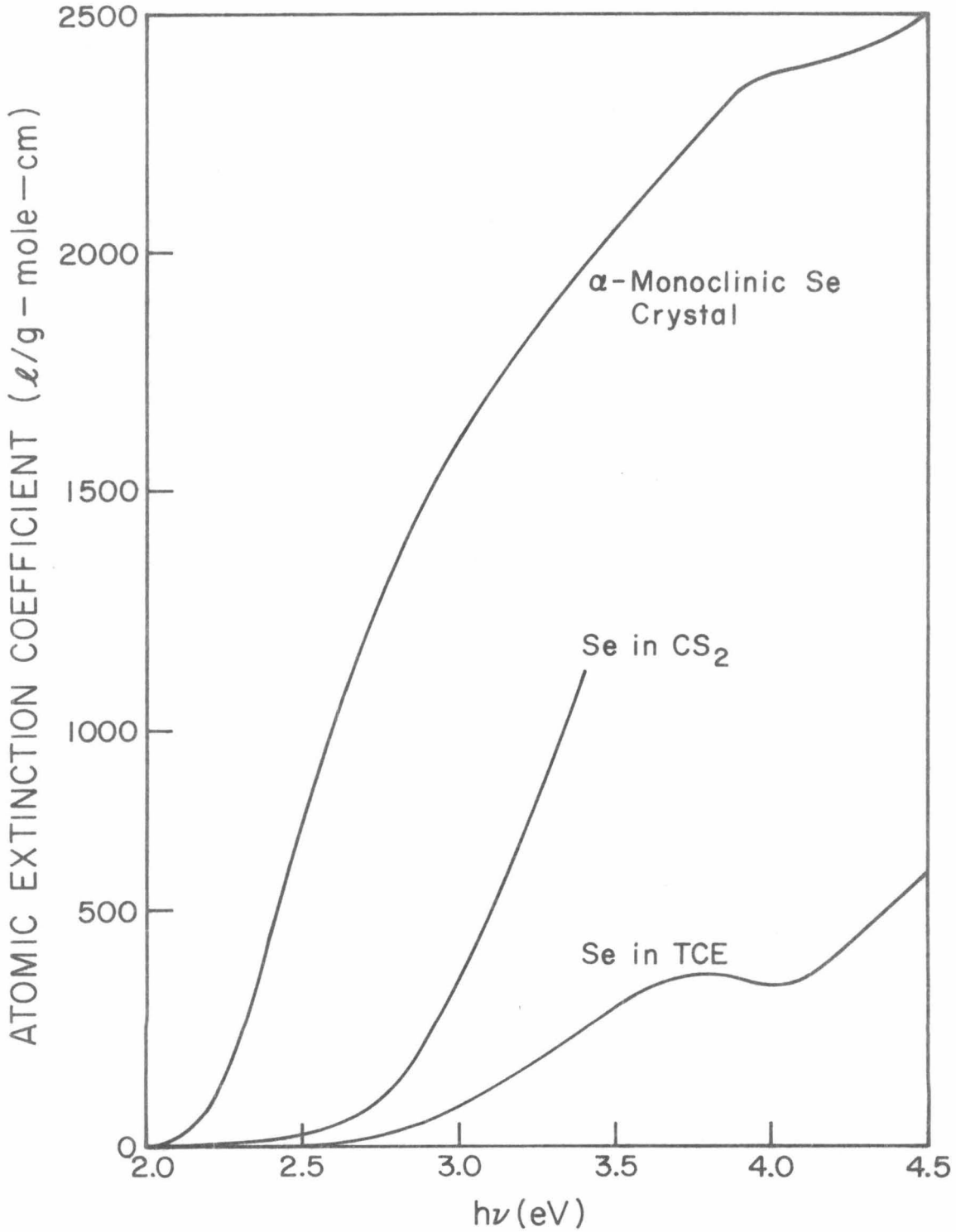

Figure 4.4 Atomic extinction coefficient for selenium in the α-monoclinic crystal, in solution in CS_2 and in trichlorethylene.

The atomic extinction coefficient of the α-monoclinic crystal is also plotted in Fig. 4.4 for comparison with the solution results.

Concerning the plot of extinction coefficient for selenium in CS_2, earlier workers have reported different results[4.8]. However, CS_2 begins to absorb strongly in the vicinity of 3·25 eV. It was found that because of this, special care had to be taken to obtain meaningful results in this region. The same coefficient was measured for a solution of approximately 1/5 the concentration used for the CS_2 measurement in Fig. 4.4. This indicates there is no appreciable concentration effect for the level of concentration used here (about 0.4 weight percent selenium in CS_2).

The plot of atomic extinction coefficient for selenium in TCE is lower than that for selenium in CS_2, but quite similar. Both give absorption edges of 2.75 eV, significantly higher than for the α-monoclinic crystal (2.20 eV). The data for toluene were qualitatively similar to that for TCE. However, there was so little selenium in the toluene solution that the measured absorption was very low. The toluene data were not included.

4.3.3 Platelets at Low Temperatures

Plots of the absorption coefficient are shown in Fig. 4.5 for three temperatures ($300^{\circ}K$, $80^{\circ}K$, $10^{\circ}K$). $300^{\circ}K$ corresponds to room temperature. The $80^{\circ}K$ temperature was measured with the germanium thermometer with liquid nitrogen ($\sim 77^{\circ}K$) in the cold chamber of the cryoflask. Similarly, the $10^{\circ}K$ was measured with liquid helium ($4.2^{\circ}K$) in the chamber. The $300^{\circ}K$ curve has been positioned with the aid of

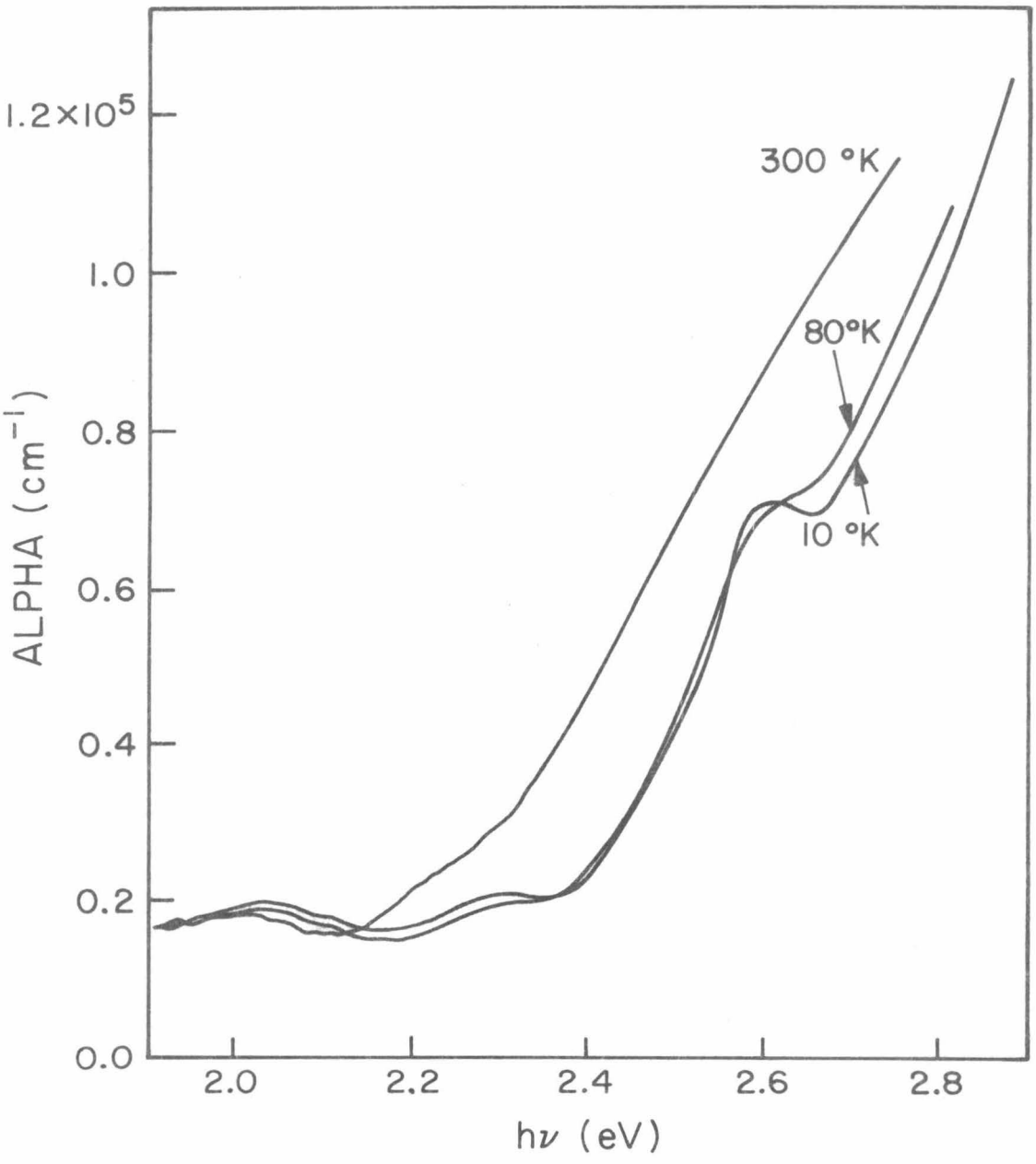

Figure 4.5 Absorption coefficient for α-monoclinic selenium 300°K, 80°K, and 10°K. Actually -ln (transmission)/ thickness. 300°K curve corrected vertically for reflection.

the transmission calculated from Appendix B, using Prosser's optical constants[4.5] at $h\nu = 2.09$ eV. The optical constants are not known for the two low temperatures, so those curves were shifted to coincide with the 300°K curve at 1.91 eV, where the measurements begin.

The first notable difference between the curves is the shift in absorption edge. From about 2.20 eV at 300°K, the edge shifts by about 0.18 eV (to 2.38 eV) at 80°K and by about 0.19 eV (to 2.39 eV) at 10°K.

The second difference occurs at about 2.65 eV. The 300°K curve is relatively straight; the 80°K curve has an inflection point at 2.64 eV; the 10°K curve has a definite maximum at 2.61 eV and a definite minimum at 2.66 eV. The 80°K and 10°K curves are quite similar, except for the behavior around 2.65 eV.

The absorption coefficient was measured as a function of polarization. At room temperature, no polarization dependence was seen. However, at 80°K, the behavior in the vicinity of 2.65 eV, is strongly polarization dependent. Fig. 4.6 shows the absorption coefficient for 6 polarizations, 30° apart. The curves are shifted vertically to separate them. The vertical scale is for the lowest curve (The exact vertical positioning of the lowest curve is somewhat arbitrary, since the optical parameters are known neither for 80°K nor as a function of polarization.). The number next to each curve is the inclination in degrees of the electric field vector with respect to the b axis of the crystal.

The curves are quite similar except for the behavior around 2.65 eV. The inflection point is resolved into two different absorption maxima,

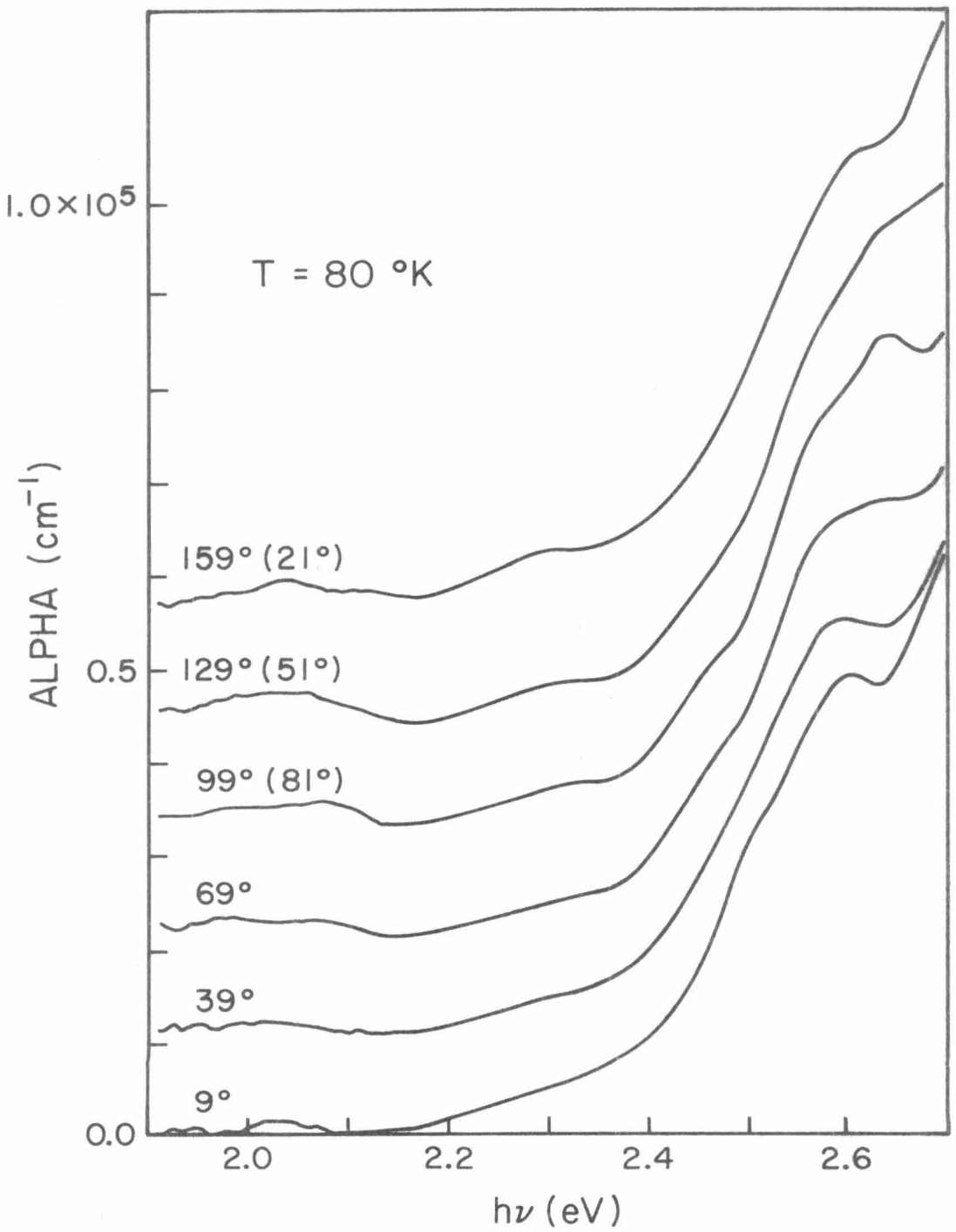

Figure 4.6 Absorption coefficient for α-monoclinic selenium at 300°K for 6 polarizations for the electric field vector relative to the crystal b axis. Curves displaced vertically for visual separation.

the 9^{o} polarization curve maximum occurring at 2.60 eV; the 99^{o} maximum, at 2.64 eV. These two curves alone, if added together, will produce an inflection point much like the one observed for non-polarized light.

Fig. 4.7 shows a portion of the 9^{o} and 99^{o} polarization curves at $80^{o}K$ and also at $10^{o}K$. The maximum and minimum is much sharper for the 9^{o} polarization curve at $10^{o}K$ than at $80^{o}K$. The 99^{o} polarization curve at $10^{o}K$ shows a much more abrupt change of slope, although the maximum at 2.64 eV remains basically unchanged. The change is probably less abrupt. Since the bandwidth of the monochromator output was 20A (corresponding to about 0.01 eV), points were measured 25A apart. Since there was very little light transmitted, greater resolution could not be attained (by decreasing the slits). These curves were not extended to higher energies because the transmitted light was insufficient. In addition to absorption, the polarizer only passes a portion of the incident light. Also, above 2.5 eV, the monochromator output decreases (the gratings being blazed at 5000 A).

4.4 Discussion

The absorption edge for selenium under various conditions is presented in Table 4.1. The edge shifts as a function of temperature, and of concentration (dense crystal vs. dilute solution). The form (or forms) in which selenium exists in solution is not known. However, it seems reasonable that it exists at least in part as Se_8 rings (discussed later). Thus, the solution absorption may be considered absorption of unperturbed rings, with an edge at 2.75 eV. To form the

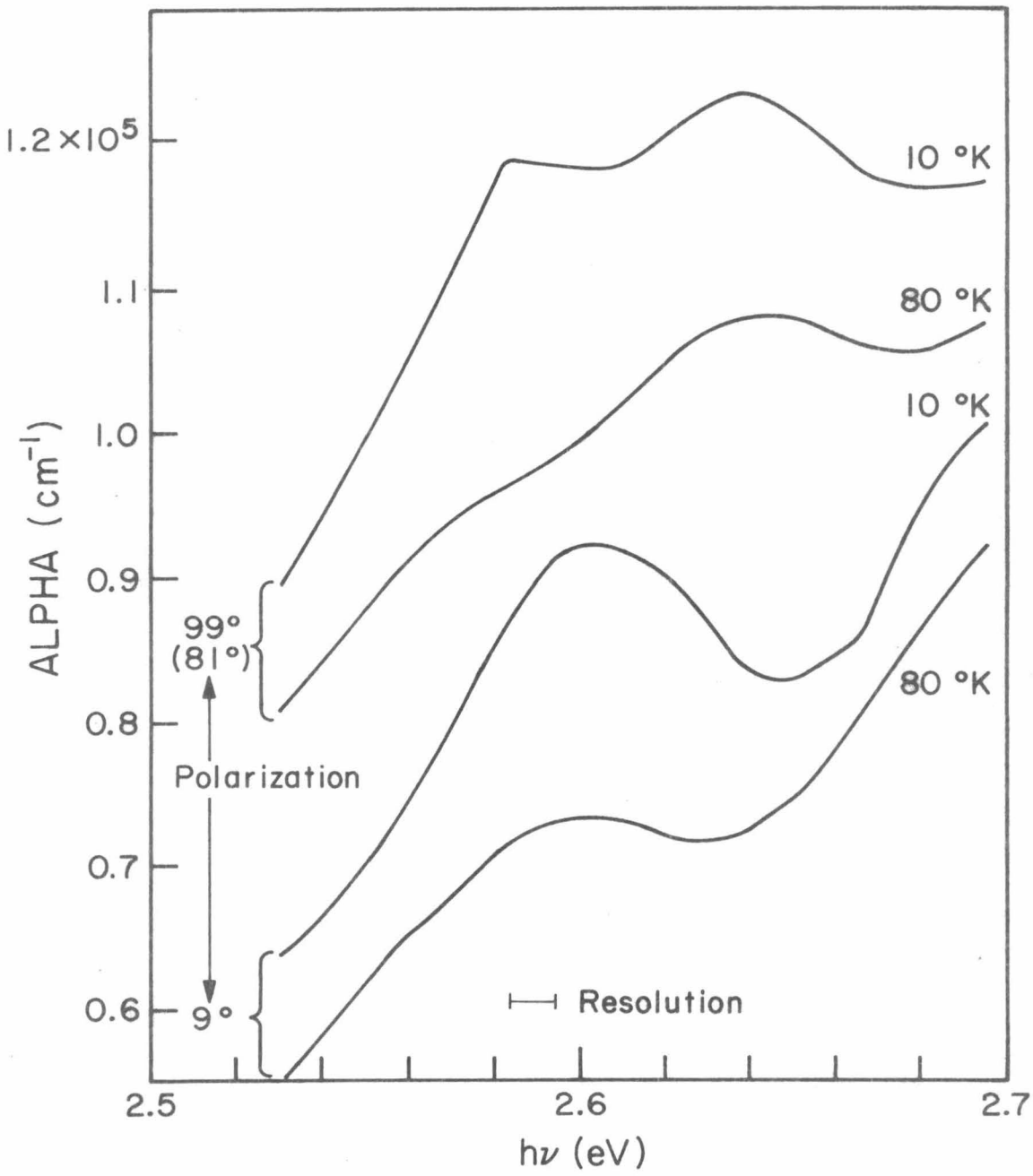

Figure 4.7 Absorption coefficient for α-monoclinic selenium for two polarizations of the electric field vector relative to the crystal b axis, for 80°K and 10°K.

TABLE 4.1

ABSORPTION EDGE OF SELENIUM UNDER VARIOUS CONDITIONS

Selenium Condition	Temperature (^{o}K)	Absorption Edge (eV)
α-monoclinic crystal	~ 300^{o}K	2.20
	80^{o}K	2.38
	10^{o}K	2.39
Selenium in CS_2	~ 300^{o}K	2.75
Selenium in TCE	~ 300^{o}K	2.75

α-monoclinic crystal, the rings must be brought together until the nearest neighbors in adjacent rings are only 3.53 A apart (The intra-ring nearest neighbor distance is 2.35 A.)[4.9]. The rings are perturbed in the α-monoclinic form, with not all bond lengths and angles the same. Thus, the proximity of the rings causes them to interact, perturbing the shape of the rings, and shifting the absorption edge to 2.20 eV (from 2.75 eV).

The two solution curves (selenium in CS_2 and TCE), while giving the same absorption edge, do <u>not</u> give the same extinction coefficient curve. Simple dilution of already widely separated molecules does not account for it (A CS_2 solution diluted to 1/5 initial concentration yielded the same curve as the initial solution.). However, the selenium may exist in solution as several species, with only one (the Se_8 ring, perhaps) contributing to absorption in this energy range. If the contributing species exists in different proportions in the two solvents, this would account for the difference between the two solution curves, while the absorption edge would be the same.

There is reason to believe that the selenium exists in several molecular species in solution, and that one of them is the Se_8 ring. If one takes a saturated solution of selenium in CS_2 and places several drops on a microscope slide, the CS_2 will evaporate in about one minute leaving behind platelets of α-monoclinic selenium with dimensions of the order of 50μ, in addition to what appear to be amorphous globs. However, the thermodynamically stable crystalline form at room temperature and atmospheric pressure is the trigonal, which is composed of

helical chains. The fact that α-monoclinic crystals precipitate from the CS_2 solution indicates that this is a kinetic process which deposits the molecules in the form in which they exist in the solution (i.e. Se_8). The same experiment with Se dissolved in TCE yields small α-monoclinic crystals. But a much larger proportion of the selenium is deposited in amorphous globs than is the case with CS_2 solutions. This indicates the TCE solution contains a smaller proportion of Se_8 than the CS_2 solution, if the inference regarding the presence of Se_8 is correct. However, the extinction coefficient curve for the CS_2 solution is significantly below the one for the α-monoclinic crystal. This indicates either the selenium is only partially in Se_8 in CS_2, or that the proximity perturbation mentioned earlier is very great indeed.

In addition, there is a definite maximum at about 3.8 eV in the extinction coefficient curve for selenium in TCE (Fig. 4.4). This is at the same energy as a slope change in the α-monoclinic curve, indicating the same process is taking place in the crystal and the solution. This is either an atomic transition, or a molecular one indicating the same molecular species (the Se_8 ring) is present in the crystal and the solution.

There is also a shift in the absorption edge between room temperature (~ $300^{o}K$) and $80^{o}K$. Fig. 4.5 shows the absorption edge to be shifted by about 0.2 eV, while the slope of the absorption coefficient curve remains nearly the same. This gives a temperature coefficient of about 8×10^{-4} $eV/^{o}K$, the same magnitude as has been reported for silicon

and germanium[4.10].

Another interesting feature at low temperatures is the polarization dependence of the absorption in the vicinity of 2.65 eV. This is shown in Fig. 4.6. Two separate minima occur, several hundreths of an eV apart for polarizations approximately parallel and normal to the b axis (the two-fold rotation axis of the crystal). The structure of the absorption curves is cleaner in Fig. 4.7, where two polarizations are explored at 80°K and 10°K (The horizontal bar represents the bandpass of the optical system, 20 A or 0.01 eV.).

The 9° polarization curve is for electric field vector nearly parallel to the crystal b axis, approximately normal to the plane of the rings. The dielectric constant along this direction is 6.06 (Chapter III). The 99° polarization curve, approximately parallel to the plane of the rings, corresponds to a dielectric constant of about 8.75. If platelets could be prepared with the (010) face instead of the (101) face predominating, the electric field vector could be polarized parallel to the plane of the rings. This would correspond to a polarization normal to the (101) plane, and cannot be done for the only orientation of platelet available (see Fig. 3.8).

CONCLUSION

The growth of α-monoclinic crystals has been discussed, and a simple method devised for identifying and orienting the crystals. The validity of this method has been confirmed by x-ray studies. In addition to bulky crystals, very thin platelets of α-monoclinic selenium have been grown.

The experimentally determined density, previously in conflict with the value calculated from accurately known crystal unit cell parameters, was carefully remeasured. Checking the procedure by measuring the density of amorphous selenium, the new value for α-monoclinic selenium ($4.389 \pm .015$ g/cm^3) is quite close to the x-ray value ($4.401 \pm .016$ g/cm^3). The technique of displacement weighing is not new, but several features are noteworthy. These include factors in the choice of a liquid and the use of a low vapor pressure liquid atop the displaced liquid to stabilize the temperature. The previously reported results, unreasonably high, may have resulted from measurements on α-monoclinic selenium partially converted to the trigonal form.

Previous reported dielectric constant measurements have not been in agreement. An apparatus was designed to reduce the effects of errors inherent in the work of the previous investigators. A two parameter model for the dielectric constant was derived, based on the similar molecular ring structure of orthorhombic sulfur. The model works quite well for the sulfur, but not as well for α-monoclinic selenium. On the basis of the measured relative dielectric constant

values and the model, the three principal axis values are:

$$\epsilon_a = 8.93 \pm .34$$

$$\epsilon_b = 6.06 \pm .49$$

$$\epsilon_c = 8.52 \pm .36$$

The thin crystal platelets were used to extend optical transmission measurements from 2.09 eV to 4.5 eV, well beyond the room temperature absorption edge of 2.20 eV. Measurements on selenium dissolved in carbon disulfide and trichlorethylene show an absorption edge of 2.75 eV, interpreted as the absorption edge of the unperturbed Se_8 rings. The rings in the crystal are perturbed physically, as shown by x-ray measurements, indicative of perturbation of the electronic states as well. The lower value of atomic extinction coefficient in the solution cases relative to the crystal indicates not all the selenium in solution contributes to the absorption. The measurements at liquid nitrogen temperature ($\sim 80^{\circ}K$) show the absorption edge is shifted from 2.20 eV to 2.38 eV, and the absorption shows an inflection point around 2.65 eV. Measurement of absorption for various polarizations of incident light show two absorption maxima about 0.04 eV apart for polarizations approximately parallel and normal to the crystal's b axis. The polarization dependence is further resolved by measurements at liquid helium temperature ($\sim 10^{\circ}K$). At that temperature the unpolarized absorption shows a well defined maximum and minimum near 2.65 eV, which appears only as an inflection point for liquid nitrogen temperature.

APPENDIX A

A COMPUTER PROGRAM FOR THE CALCULATION OF ANGLES BOUNDING CRYSTAL FACES

The angles formed by edges of crystal faces can be related to the parameters of the unit cell of the crystal. An edge corresponds to an intersection of two crystal planes. A face angle corresponds to two crystal planes intersecting in a third plane.

Crystal planes are designated by Miller indices. A Miller index is an ordered triple, each number of which is the reciprocal of that plane's incept of the crystal axis, in units of the length of that crystal axis. The index is expressed as integers. Thus, a plane whose axis intercepts are $(2a, b, \infty)$ has a Miller index of (120), the plane being parallel to the c axis (intercept of ∞).

Using the parameters of the unit cell, and choosing the crystal planes to be investigated, face angles can be calculated. First, each Miller index is converted to a vector, normal to that plane in x-y-z space. Three planes (normal vectors) are chosen. One plane is chosen as the base plane, representing the crystal face. The cross products of the two other vectors with the vector of the base plane are vectors whose directions are the lines of intersection within the base plane. These vectors are normalized to unit length. The dot product of these normalized vectors is the cosine of the angle of intersection within the base plane.

This program can be run with monoclinic, orthorhombic, tetragonal, hexagonal and cubic crystals. All three crystal axis lengths must be supplied, even if they are equal. Also, the planes to be considered must be supplied. For triclinic crystals, the crystal data input statements must be modified to accept 3 angles, and the conversion from Miller index to unit normal in x-y-z space must be modified.

In addition, the number of planes must be entered, and the number of cases this implies. There are N(N-1)(N-2)/6 ways to choose a combination of three things from a group of N without replacement. For each choice of three planes, each plane may be considered the base plane, so the number of cases is N(N-1)(N-2)/2. This can become unwieldy quickly. For planes (for monoclinic crystals) with 1,0,-1 in the Miller indices, there are 13 non-equivalent planes (Table A.1). This gives 858 cases. For planes (for monoclinic crystals) with 2,1,0,-1,-2, there are 49 planes (Table A.2) which give 55,272 cases.

Specific program information:

1. The program was run on an IBM 360/75 computer. Time for 858 cases was 7 sec. Time for 1365 cases was 13 sec. Memory for program and 858 cases was 21,000. Remember: There are 4 arrays NT long.
2. Dimension statement: The arrays AN, IDX, INDEX, INDEX1 must be dimensioned to the number of cases or larger, which is given by N(N-1)(N-2)/2, where N is the number of planes.

TABLE A.1

NON-EQUIVALENT PLANES FOR MONOCLINIC CRYSTALS

WITH + 1,0,-1 IN THE MILLER INDEX

100	110	111
010	$1\bar{1}0$	$11\bar{1}$
001	101	$1\bar{1}1$
	$10\bar{1}$	$\bar{1}11$
	011	
	$01\bar{1}$	

TABLE A.2

NON-EQUIVALENT PLANES FOR MONOCLINIC CRYSTALS

WITH +2, +1,0,-1,-2 IN THE MILLER INDEX

$2\,1\,0$	$2\,1\,1$	$2\,2\,1$	$1\,0\,0$
$2\,\bar{1}\,0$	$2\,1\,\bar{1}$	$2\,2\,\bar{1}$	$0\,1\,0$
$1\,2\,0$	$2\,\bar{1}\,1$	$2\,\bar{2}\,1$	$0\,0\,1$
$1\,\bar{2}\,0$	$\bar{2}\,1\,1$	$\bar{2}\,2\,1$	$1\,1\,0$
$2\,0\,1$	$1\,2\,1$	$2\,1\,2$	$1\,\bar{1}\,0$
$2\,0\,\bar{1}$	$1\,2\,\bar{1}$	$2\,1\,\bar{2}$	$1\,0\,1$
$1\,0\,2$	$1\,\bar{2}\,1$	$2\,\bar{1}\,2$	$1\,0\,\bar{1}$
$1\,0\,\bar{2}$	$\bar{1}\,2\,1$	$\bar{2}\,1\,2$	$0\,1\,1$
$0\,2\,1$	$1\,1\,2$	$1\,2\,2$	$0\,1\,\bar{1}$
$0\,2\,\bar{1}$	$1\,1\,\bar{2}$	$1\,2\,\bar{2}$	$1\,1\,1$
$0\,1\,2$	$1\,\bar{1}\,2$	$1\,\bar{2}\,2$	$1\,1\,\bar{1}$
$0\,1\,\bar{2}$	$\bar{1}\,1\,2$	$\bar{1}\,2\,2$	$1\,\bar{1}\,1$
			$\bar{1}\,1\,1$

3. Data - crystal parameters. The first data card contains A,B,C, BETA1, BETA2. Each is allocated 10 spaces on first data card: A has 1-10, B has 11-20, etc. There must be a decimal point in each number. A,B,C, are the lengths of the crystal axes, BETA1 and BETA2 are the degrees and minutes part of the angle opposite the b axis.

4. Data - number of planes and cases. The second data card contains N, the number of planes considered, and NT, the total number of cases, given by N(N-1)(N-2)/2. N is a 2 digit integer located in columns 9 and 10 of the card. If N = 9 or less, it must be in column 10. NT is a 7 digit integer in columns 14 - 20. Its last digit must be in column 20.

5. Data - crystal planes. The remaining data cards contain the Miller indices of the planes considered, 10 to a card, allowing 8 columns per index. 1 and 2, 3 and 4, 5 and 6 contain the 3 numbers of the index, including (-) sign where needed. 7 and 8 are blank. The integer itself must be in column 2,4,6. 1,3,5 are for signs. Thus, the first part of the indices appear in columns 1 and 2, 9 and 10, 17 and 18, etc.

The program follows.

```
C     PROGRAM TO FIND ANGLES TWO CRYSTAL PLANES MAKE BY INTERSECTING IN A THIRD
C     PLANE, TO BE USED IN IDENTIFYING CRYSTAL FACES AND ORIENTATIONS.
C     THIS PROGRAM CAN BE USED WITH MONOCLINIC AND HIGHER SYMMETRY CRYSTALS.
C     TO WORK WITH TRICLINIC CRYSTALS, THE SECTION ON CONVERTING MILLER INDICES
C     TO X Y Z COORDINATE SYSTEM MUST BE MODIFIED, AS WELL AS THE READ
C     INSTRUCTION AND FORMAT FOR THE CRYSTAL PARAMETERS.
C     ARRAYS AN,IDX,INDEX,INDEX1 MUST BE DIMENSIONED TO NUMBER OF CASES NI.
C     GIVEN BY N*(N-1)*(N-2)/2 WHERE N IS THE NUMBER OF PLANES CONSIDERED.
      DIMENSION AN(1365),IDX(1365),INDEX(1365),INDEX1(1365)
C     DIMENSION OTHER ARRAYS.  THE 50 MUST BE INCREASED IF MORE THAN THAT MANY
C     CRYSTAL PLANES ARE TO BE TREATED.  THIS IS VERY UNLIKELY.
      DIMENSION D(3,3),E(3,3),Y(3),Z(3),I(50),J(50),K(50),V(50,3)
C     A,B,C ARE LENGTHS OF CRYSTAL AXES.  UNITS ARE IRRELEVANT.
C     BETA1,BETA2 - MONOCLINIC ANGLE IN DEGREES AND MINUTES.  BOTH MUST BE
C     ENTERED, EVEN IF BETA2 IS ZERO.  OTHER ANGLES MUST BE INCLUDED FOR
C     TRICLINIC CRYSTALS.  READ AND FORMAT MUST BE CHANGED, NEW VARIABLES ADDED.
      READ(5,101)A,B,C,BETA1,BETA2
  101 FORMAT(8F10.5)
C     NUMBER OF PLANES AND CASES MUST BE ENTERED.
      READ(5,102)N,NT
  102 FORMAT(8X,I2,3X,I7)
C     CRYSTAL PLANES ARE READ, GIVEN BY MILLER INDICES.
      READ(5,103)(I(L),J(L),K(L),L=1,N)
  103 FORMAT(10(3I2,2X))
      PI=4.0*ATAN(1.0)
      BETA3=(BETA1+BETA2/60.)*PI/180.0
C     IN IS A COUNTER, COUNTING THE NUMBER OF CASES COMPUTED, NEEDED FOR SORT.
      IN=0
C     MILLER INDICES AND CRYSTAL DATA CONVERTED TO X Y Z COORDINATE SYSTEM.
C     THE V ARRAY CONSISTS OF VECTORS NORMAL TO THE APPROPRIATE PLANE.
      DO 10 L=1,N
      V(L,1)=FLOAT(I(L))/A
      V(L,2)=FLOAT(J(L))/B
   10 V(L,3)=(FLOAT(K(L))-V(L,1)*C*COS(BETA3))/(C*SIN(BETA3))
C     THREE CRYSTAL PLANES CHOSEN TO WORK WITH.
      NM1=N-1
      NM2=N-2
      DO 50 I1=1,NM2
      DO 20 IP=1,3
   20 D(1,IP)=V(I1,IP)
      M1=I1+1
      DO 50 J1=M1,NM1
      DO 21 IP=1,3
   21 D(2,IP)=V(J1,IP)
      M2=J1+1
      DO 50 K1=M2,N
      DO 22  IP=1,3
   22 D(3,IP)=V(K1,IP)
C     CROSS PRODUCTS ARE TAKEN, TO GET VECTORS WHICH REPRESENT THE LINE OF
C     INTERSECTION BETWEEN THE BASE PLANE AND AN INTERSECTING PLANE.  TWO OF
C     THESE VECTORS WILL BE NORMALIZED AND THE DOT PRODUCT TAKEN TO FIND THE
C     COSINE OF THE INTERSECTION ANGLE.  FINALLY THE INVERSE COSINE IS TAKEN.
      DO 25 IP=1,3
      I2=IP+1
      IF(IP.EQ.3) I2=1
      E(IP,1)=D(IP,2)*D(I2,3)-D(I2,2)*D(IP,3)
      E(IP,2)=D(IP,3)*D(I2,1)-D(I2,3)*D(IP,1)
   25 E(IP,3)=D(IP,1)*D(I2,2)-D(I2,1)*D(IP,2)
      DO 26 IP=1,3
      P=E(IP,1)**2+E(IP,2)**2+E(IP,3)**2
      IF(P.LT.1.0E-5) P=0.0
```

```
   26 Z(IP)=SQRT(P)                                                    62
C     CROSS PRODUCTS NORMALIZED.                                       63
      DO 30 IP=1,3                                                     64
      DO 30 IQ=1,3                                                     65
      IF(Z(IP).LE.0.0) GO TO 29                                        66
      E(IP,IQ)=E(IP,IQ)/Z(IP)                                          67
      GO TO 30                                                         68
   29 E(IP,IQ)=0.0                                                     69
   30 CONTINUE                                                         70
C     DOT PRODUCTS TAKEN.  COSINE OF ANGLE AND ANGLE FOUND.            71
      DO 36 IP=1,3                                                     72
      IQ=IP+1                                                          73
      IF(IP.EQ.3) IQ=1                                                 74
      IF(Z(IP).LE.1.0E-5) GO TO 34                                     75
      Q=ABS(E(IP,1)*E(IQ,1)+E(IP,2)*E(IQ,2)+E(IP,3)*E(IQ,3))           76
      IF(Q.GT.1.0E-5) GO TO 33                                         77
      Y(IP)=PI/2.0                                                     78
      GO TO 36                                                         79
   33 W=1.0-Q*Q                                                        80
      W=ABS(W)                                                         81
      IF(W.GE.1.0) GO TO 35                                            82
      Y(IP)=ATAN(SQRT(W)/Q)                                            83
      GO TO 36                                                         84
   34 Y(IP)=0.0                                                        85
      GO TO 36                                                         86
   35 Y(IP)=0.0                                                        87
   36 CONTINUE                                                         88
C     ARRAY CALLED INDEX IS MADE UP CONTAINING THE CRYSTAL PLANES CODED FOR  89
C     LATER IDENTIFICATION.                                            90
      DO 40 IP=1,3                                                     91
      IQ=IP+1                                                          92
      IN=IN+1                                                          93
      IF(IP.EQ.3) IQ=1                                                 94
      INDEX(IN)=100000*I1+1000*J1+10*K1+IQ                             95
   40 AN(IN)=Y(IP)                                                     96
   50 CONTINUE                                                         97
C     ANGLES AND IDENTIFICATION SORTED BY DECREASING ANGLE.            98
      CALL SORTD2(AN,IN,IDX)                                           99
      DO 55 IP=1,IN                                                   100
      KK=IDX(IP)                                                      101
   55 INDEX1(IP)=INDEX(KK)                                            102
C     HEADING FOR OUTPUT IS WRITTEN.                                  103
      WRITE(6,201)                                                    104
  201 FORMAT(1H1,14H SORTED ANGLES  .///)                             105
C     ANGLES CONVERTED TO DEGREES AND MINUTES.  SUPPLEMENT ALSO FOUND. 106
      DO 60 IP=1,IN                                                   107
      X1=180.0*AN(IP)/PI                                              108
      X2=180.0-X1                                                     109
      IX1=X1                                                          110
      IX2=X2                                                          111
      X11=60.0*(X1-FLOAT(IX1))                                        112
      X21=60.0*(X2-FLOAT(IX2))                                        113
      NZ=INDEX1(IP)-10*(INDEX1(IP)/10)                                114
      LA=INDEX1(IP)/100000                                            115
      LB=INDEX1(IP)/1000-100*LA                                       116
      LC=INDEX1(IP)/10-10000*LA-100*LB                                117
      IF(NZ-2) 56,57,58                                               118
   56 L1=LA                                                           119
      L2=LB                                                           120
      L3=LC                                                           121
      GO TO 59                                                        122
```

```
   57 L1=LR                                                              123
      L2=LC                                                              124
      L3=LA                                                              125
      GO TO 59                                                           126
   58 L1=LC                                                              127
      L2=LA                                                              128
      L3=LR                                                              129
C     LINE OF OUTPUT IS WRITTEN, ANGLE AND SUPPLEMENT IN DEGREES AND MINUTES,  130
C     THEN MILLER INDICES OF BASE PLANE AND TWO INTERSECTING PLANES.       131
   59 WRITE(6,202) IX1,X11,IX2,X21,I(L1),J(L1),K(L1),I(L2),J(L2),K(L2),    132
     1I(L3),J(L3),K(L3)                                                    133
  202 FORMAT(1H ,2(I3,2X,F7.2,3X),5X,3(3I2,2X))                          134
   60 CONTINUE                                                           135
      STOP                                                               136
      END                                                                137
                                                                         138
                                                                         139
```

APPENDIX B

TRANSMISSION OF LIGHT THROUGH TWO DISSIMILAR MEDIA

In attempting to unravel the transmission data, the problem arises of finding the fraction of incident light which is transmitted through a structure composed of 2 layers of dissimilar material. It is a four layer problem with three interfaces. This problem may be solved in a straightforward, if tedious, manner by requiring the solution of the wave equation and its derivative to match at all three interfaces. Under the simplifying assumption of no absorption in the second layer (e.g. the quartz substrate) the solution reduces to

$$T = 16/[G_1 + G_2 \cos(4\pi n_2 a/\lambda) + G_3 \sin(4\pi n_2 a/\lambda)] \qquad (B.1)$$

where T is the ratio of transmitted to incident power, a is the thickness of the second layer, n_2 is the index of refraction of the second layer, and λ is the free space wavelength of the incident light. The G's are defined by:

$$\begin{aligned} G_1 = {} & (A_1^2 - A_2^2 - A_3^2 - A_4^2 - A_5^2 + A_6^2) \cos(4\pi nd/\lambda) \\ & + 2(A_1A_5 + A_3A_6) \sin(4\pi nd/\lambda) \\ & + 2(A_1A_4 + A_2A_6) \sinh(4\pi kd/\lambda) \\ & + (A_1^2 + A_2^2 + A_3^2 + A_4^2 + A_5^2 + A_6^2) \\ & \times \cosh(4\pi kd/\lambda) \end{aligned} \qquad (B.2a)$$

$$G_2 = (A_1^2 + A_2^2 + A_3^2 - A_4^2 - A_5^2 - A_6^2) \cos (4\pi nd/\lambda)$$
$$+ 2(A_1A_5 - A_3A_6) \sin (4\pi nd/\lambda)$$
$$+ 2(A_1A_4 - A_2A_6) \sinh (4\pi kd/\lambda)$$
$$+ (A_1^2 - A_2^2 - A_3^2 + A_4^2 + A_5^2 - A_6^2)$$
$$\times \cosh (4\pi kd/\lambda) \qquad \text{(B.2b)}$$

$$G_3 = 2(A_2A_5 - A_3A_4) \cos (4\pi nd/\lambda)$$
$$+ 2(A_4A_6 - A_1A_2) \times \sin (4\pi nd/\lambda)$$
$$+ 2(A_3A_4 - A_2A_5) \cosh (4\pi kd/\lambda)$$
$$+ 2(A_1A_3 - A_5A_6) \sinh (4\pi kd/\lambda) \qquad \text{(B.2c)}$$

where n and k are respectively the real and imaginary parts of the index of refraction of the first (e.g. selenium) layer, d is the thickness of this layer and

$$A_1 = 2 \qquad \text{(B.3a)}$$

$$A_2 = n(n_2^2 + n^2 + k^2)/n_2(n^2 + k^2) \qquad \text{(B.3b)}$$

$$A_3 = k(n^2 + k^2 - n_2^2)/n_2(n^2 + k^2) \qquad \text{(B.3c)}$$

$$A_4 = n(n^2 + k^2 + n_0^2)/n_0(n^2 + k^2) \qquad \text{(B.3d)}$$

$$A_5 = k(n^2 + k^2 - n_0^2)/n_0(n^2 + k^2) \qquad \text{(B.3e)}$$

$$A_6 = (n_2^2 + n_0^2)/n_0 n_2 \tag{B.3f}$$

and n_0 is the index of the initial surrounding media.

The question arises of how to handle the sinusoidal terms of argument $4\pi na/\lambda$ in Eq. B.1. Since the monochromator has a bandpass of about 10-20 A in the configuration in which it was used, the bandpass must be averaged over. Defining $\Delta\lambda$ to be the bandpass and λ_0 to be the nominal wavelength one obtains

$$T \cong 16/G_1 \left[1 + ((G_2^2 + G_3^2)/G_1^2)^{1/2} \cos (4\pi n_0 a\Delta\lambda/\lambda_0^2 + \theta)\right] \tag{B.4}$$

where θ is a quantity which does not vary during the averaging. Then $\langle T\rangle = \int T d(\Delta\lambda)/\int d(\Delta\lambda)$, but since the argument of the cos goes through many cycles

$$\langle T\rangle \cong \frac{N\int_0^{2\pi} \{16(G_1)^{-1}[1 + (G_2^2 + G_3^2)/G_1^2)^{1/2}\cos\varphi]^{-1} \, d\varphi\}}{N\int_0^{2\pi} d\varphi} \tag{B.5}$$

because the integral over a partial cycle is small with respect to the integral over many cycles. Therefore,

$$\langle T\rangle \cong \frac{16}{G_1\left[1 - ((G_2^2 + G_3^2)/G_1^2)\right]^{1/2}} \tag{B.6}$$

The cos φ term of Eq. (B.6) does not average to zero.

$$\frac{d\varphi}{1 + a\cos\varphi} = d\varphi\,(1 - a\cos\varphi + a^2\cos^2\varphi + \ldots) \quad 0 \le a < 1 \tag{B.7}$$

While the odd order terms average to zero over a cycle as expected, the even order terms are always positive. The magnitude of the effect of the correction term, $(G_2^2 + G_3^2)/G_1^2$, is at most several percent. While this is small enough to justify the approximation, it is large enough to affect calculated values of n and k.

APPENDIX C

DISCUSSION OF THE RELATIONSHIP BETWEEN THE DIELECTRIC CONSTANT AND OPTICAL CONSTANTS

The dielectric tensor of Chapter III is insufficient to describe the interaction of electromagnetic fields with a crystal. To account for absorption, complex dielectric constants or a conductivity tensor (σ) must be introduced[C.1]. In this way, losses can be dealt with. For orthorhombic and higher symmetry crystals, the principal axes of the dielectric and conductivity tensors coincide, simplifying the analysis.*

Taking the coordinate axes in the directions of the principal tensor axes, and introducing complex quantities:

$$\hat{\varepsilon}_m = \varepsilon_m + 4\pi i\, \sigma_m/\omega \quad (m = x,y,z) \tag{C.1}$$

where the $\hat{}$ indicates a complex quantity, m is a principal axis direction and ω is the angular frequency of the electromagnetic field. Similarly, for the refractive index:

$$\hat{n} = n + i\,k \tag{C.2}$$

where k is the extinction coefficient. But:

$$\hat{n} = \sqrt{\mu\hat{\varepsilon}} \tag{C.3}$$

---

*Since its a and c axes are only 46' from being orthogonal, considering α-monoclinic selenium to be orthorhombic is a good approximation.

where μ is the relative permeability, and is taken to be 1 for non-magnetic materials. Squaring Eqs. (C.2) and (C.3), substituting Eq. (C.1), and equating real and imaginary parts:

$$n_m^2 - k_m^2 = \epsilon_m \tag{C.4a}$$

$$n_m k_m = 2\pi\sigma_m/\omega \tag{C.4b}$$

Solving for n_m and k_m:

$$n_m = \epsilon_m^{1/2} \left[1/2 + \left[1/4 + \left(\frac{2\pi\sigma_m}{\omega\epsilon_m}\right)^2\right]^{1/2}\right]^{1/2} \tag{C.5a}$$

$$k_m = \epsilon_m^{1/2} \left[\left[1/4 + \left(\frac{2\pi\sigma_m}{\omega\epsilon_m}\right)^2\right]^{1/2} - 1/2\right]^{1/2} \tag{C.5b}$$

For small absorption:

$$n_m \simeq \epsilon_m^{1/2} \tag{C.6a}$$

$$k_m \simeq 2\pi\sigma_m/\omega \tag{C.6b}$$

This relates n, k, ϵ and σ, but only at a given energy.

If the function $\hat{n}$ in Eq. (C.2) has no poles in the lower (or upper) half of the complex plane, the functions n and k are related through the Kramers-Kronig relations[C.2]:

$$n(\omega) = \frac{-1}{\pi} \text{P.V.} \int_{-\infty}^{\infty} \frac{k(\omega')\, d\omega'}{\omega' - \omega} \tag{C.7a}$$

$$k(\omega) = \frac{1}{\pi} \text{P.V.} \int_{-\infty}^{\infty} \frac{n(\omega')\, d\omega'}{\omega' - \omega} \tag{C.7b}$$

where P.V. indicates that the Cauchy principle value is to be taken. Thus, if the index of refraction or the extinction coefficient is known for all frequencies, and the combined function $\hat{n}(\omega)$ has either the upper or lower half plane free of poles, the other function can be determined using Eq. (C.7).

To investigate the behavior of n and K in a limited region, however, it is only necessary to know the behavior of n or K over that region. All other poles must be sufficiently far removed that they do not contribute significantly to the integrals in Eqs. (C.7). This is equivalent to saying that there must be no absorption lines or bands other than those considered near the region of interest.

Concerning the results of chapters III and IV, a few conclusions may be drawn. Kyropoulos[C.3] determined the indices of refraction for α-monoclinic selenium for two directions, of the electric field: parallel and normal to the twofold rotation axis (see Table C.1). Considering the errors, n^2 is approximately equal to ϵ for the two directions. There appears to be no absorption in the crystal between 100Kc and optical frequencies below the absorption edge. This is quite reasonable, since α-monoclinic selenium should exhibit no ionic behavior, and it is ionic crystals which have infra-red active optical modes[C.4].

The absorption shown in Fig. 4.3 indicates several transitions in the region above 2.25eV. That there is more than one is indicated by the changes in slope of the plot of α as a function of $h\nu$.

TABLE C.1

Relationship between n and ϵ for two directions in α-monoclinic selenium.

Direction	n (Ref. C.3)	n^2	ϵ (This work)
parallel to b axis	2.3±.1	5.3±.5	6.06 ± .25
normal to b axis	2.8±.1	7.9±.6	8.73 ± .38

Concerning the dielectric anisotropy, the only observed optical anisotropy is shown in Fig. 4.6. It is so small it could not conceivably produce the dielectric anisotropy observed (6.06 and 8.73). Consider an expression for the static dielectric constant[C.5]:

$$\epsilon = 1 + (Ne^2/m\ \epsilon_o) \sum fi/\omega i^2 \qquad (C.8)$$

where N is the number of electrons involved per unit volume, e and m are the electron charge and mass respectively, ϵ_o is the permittivity of free space, fi is the oscillator strength, and ωi is the oscillator frequency. The fi can be found approximately from the height, width and frequency of the small absorption peaks in Fig. 4.6. The value of f is found to be about 0.01. Evaluating Eq. (C.8) for the two peaks, and taking the difference, the change in dielectric constant is less than 10^{-6}. Thus, the dielectric anisotropy must be caused by absorption anisotropy above 2.7eV.

A different form of Eq. (C.8) is used by experimental workers[C.6]:

$$\epsilon(\lambda) \simeq n^2\ (\lambda) = 1 + \sum_i [Si\lambda i^2/C1 - (\lambda i/\lambda)^2)] \qquad (C.9)$$

where Si and λi are the strength and wavelength of the $i^{\underline{th}}$ oscillator. This expression is valid for low absorption and is known as the Sellmeier dispersion formula.

A model may be considered as follows. Let the lower static dielectric constant (6.06) be accounted for by a number of Sellmeier oscillators in Eq. (C.9). Assume the anisotropy (8.73 - 6.06) be

accounted for by a single oscillator active in only one polarization, with the condition that the absorption at 2.7eV be perturbed by no more than 3%. While the value of 3% is somewhat arbitrary, it has been demonstrated above that at energies below 2.7eV there is little contribution to the dielectric anisotropy. An oscillator at 8.25eV with a strength of $1.06 \times 10^{14}/m^2$ will satisfy the imposed conditions, and account for the anisotropy. These values are similar to those obtained by DiDomenico and Wemple[C.6] for a wide range of materials. This means only that since there is little anisotropy below 2.7eV, one might look for an absorption anisotropy near or above 8.25eV, if the single oscillator model is correct. The model, however, only places a lower limit on the energy of the oscillator.

Alternatively, the anisotropy may be explained by a more complicated absorption anisotropy. Rutile[C.7] for example, has a dielectric anisotropy comparable to that of α-monoclinic selenium and an absorption which is isotropic below 4.0eV. Above this energy, however, the absorption is quite anisotropic.

Regardless of the actual mechanism, the dielectric anisotropy in α-monoclinic selenium can be attributed to an absorption anisotropy above 2.7eV.

REFERENCES

Chapter I

1.1 J. W. Moody and R. C. Himes, Mat. Res. Bull. 2, 703 (1967)

1.2 M. Mitscherlich, Ann. Chem. Phys. 3, 46, 301 (1856)

1.3 Handbook of Chemistry and Physics, Chemical Rubber Co., Cleveland, Ohio, 49th edition, p. B-240 (1968)

1.4 W. Muthmann, Z. Krist. 17, 336 (1890)

1.5 S. Iizima and M-A. Nicolet, JPL Space Programs Summary 37-48, vol. III, p. 70 (1967)

1.6 R. D. Burbank, Acta Cryst. 4, 140 (1951)

1.7 R. E. Marsh, L. Pauling and J. D. McCullough, Acta Cryst. 6, 71 (1953)

1.8 H. P. Klug, Z. Krist. 88, 128 (1934)

1.9 R. E. Marsh, private communication

Chapter II

2.1 R. D. Burbank, Acta Cryst. 4, 140 (1951)

2.2 S. Iizima and M-A. Nicolet, JPL Space Programs Summary, vol. III, 37-48, p. 70 (1967)

2.3 J. W. Moody and R. C. Himes, Mat. Res. Bull. 2, 703 (1967)

2.4 J. Timmermans, Physico-Chemical Constants of Pure Organic Compounds, Elsevier, New York, vol. I, p. 226 (1950), vol. II, p. 184, p. 434 (1965)

2.5 Handbook of Chemistry and Physics, Chemical Rubber Co., Cleveland, Ohio, 49th edition, B-240 (1968)

2.6 M. Mitscherlich, Ann. Chem. Phys. 3, 46, 301 (1856)

2.7 K. Rammelsberg, Pogg. Ann. 152, 151 (1874)

2.8 E. Petersen, Z. Phys. Chem. 8, 612 (1891)

2.9 A. P. Saunders, J. Phys. Chem. 4, 423 (1900)

2.10 M. Coste, C. R. 149, 674 (1909)

2.11 M. Sneed, et al, Comprehensive Inorganic Chemistry, Van Nostrand, New York, vol. VIII, p. 16 (1961)

2.12 R. E. Marsh, private communication

2.13 W. Muthmann, Z. Krist. 17, 336 (1890)

Chapter III

3.1 S. Kyropoulos, Z. Phys. 40, 618 (1927)

3.2 S. Iizima and M-A. Nicolet, JPL Space Programs Summary, vol. III, 37-48, p. 70 (1967)

3.3 J. Caywood, Optical and Electrical Properties of α-monoclinic Selenium, Ph.D. Dissertation, California Institute of Technology, Pasadena, California (1969)

3.4 B. Gudden and R. Pohl, Z. Phys. 35, 18 (1926)

3.5 S. Iizima, private communication

3.6 W. Muthmann, Z. Krist. 17, 336 (1890)

3.7 H. Pélabon, Ann. Chim. et Phys. 17, 556 (1909)

3.8 Von Hippel, editor, Dielectric Materials and Applications, Wiley, New York, p. 302 (1954)

3.9 A. M. Mood, Introduction to the Theory of Statistics, McGraw Hill, New York, p. 117 (1950)

3.10 J. Mathews and R. L. Walker, Mathematical Methods of Physics, W. A. Benjamin, Inc., New York, p. 365-367 (1965)

3.11 J. F. Nye, Physical Properties of Crystals, Clarendon Press, Oxford, p. 297 (1957)

3.12 J. Mathews and R. L. Walker, loc. cit., p. 374-380

3.13 B. E. Warren and J. T. Burwell, J. Chem. Phys. 3, 6 (1935)

3.14 Handbook of Chemistry and Physics, Chemical Rubber Co., Cleveland, Ohio, 49th edition, p. E-61 (1968)

3.15 R. D. Burbank, Acta Cryst. 4, 140 (1951)

3.16 B. Meyer, editor, Elemental Sulfur Chemistry and Physics, Interscience, New York, p. 20-22 (1965)

3.17 A. S. Cooper, W. L. Bond and S. C. Abrahams, Acta Cryst. 14, 548 (1961)

Chapter IV

4.1 R. S. Coldwell and H. Y. Fan, Phy. Rev. 114, 664 (1959)

4.2 J. J. Dowd, Proc. Phys. Soc. B64, 783 (1951)

4.3 M. A. Gilleo, J. Chem. Phys. 19, 1291 (1951)

4.4 T. S. Moss, Photoconductivity of the Elements, Butterworth, London, p. 185-203 (1952)

4.5 V. Prosser, Cs. Cas. Fys. 10, 35 (1960)

4.6 E. D. Kolb, First International Symposium Physics of Selnium and Tellurium, Program and Extended Abstracts, p. 25 (1967)

4.7 S. Iizima, private communication

4.8 J. E. Fergusson, et al., J. Inorg. Nucl. Chem. 24, 157 (1962)

4.9 R. D. Burbank, Acta Cryst. 4, 140 (1951)

4.10 T. S. Moss, loc. cit. p. 103, 115, 132

Appendix C

C.1 M. Born and E. Wolf, Principles of Optics, 3rd edition, Pergamon Press, London, p. 708 ff. (1965)

C.2 A. Yariv, Quantum Electronics, Wiley, New York, p. 130-131, p. 455-456 (1967)

C.3 S. Kyropoulos, Z. Phys. 40, 618 (1927)

C.4 C. Kittel, Introduction to Solid State Physics, 3rd edition, Wiley, New York, p. 148 ff. (1967)

C.5 G. Fowles, Introduction to Modern Optics, Holt, Rinehart and Winston, New York, Chapter 5 (1968)

C.6 M. DiDomenico and S. Wemple, J. App. Phys. 40, 720 (1969)

C.7 M. Cardona and G. Harbeke, Phy. Rev. 137, A1467 (1965)